Scatterometer

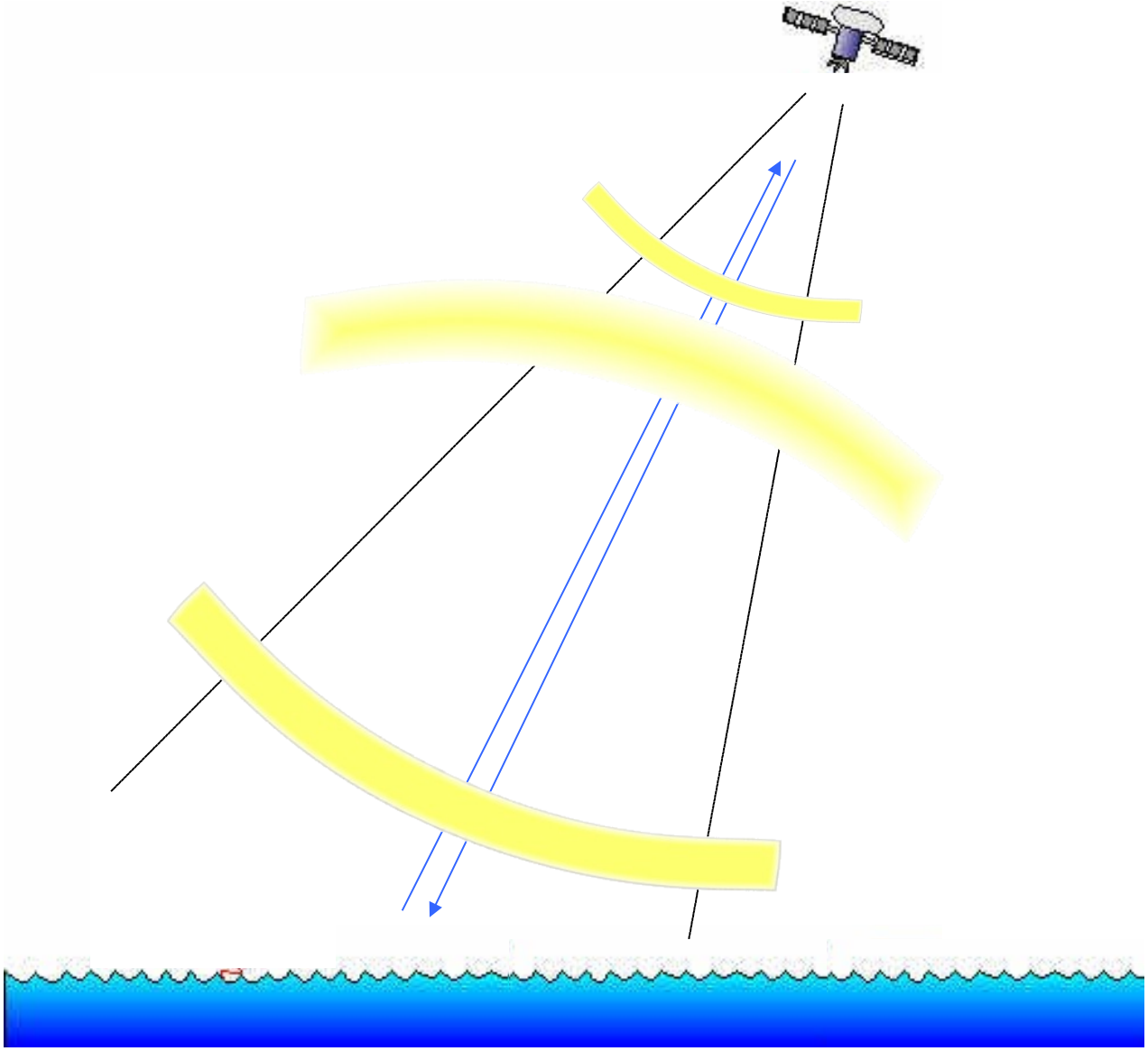

Antenna details:

Define power pattern of antenna

$$R(\Omega) = \int_A \int_{\Delta f} L_f \, dA \, df$$ Radiant Intensity Watts/Sr

$$\Phi = \int_\Omega R(\Omega) \, d\Omega$$ Watts

$$P(\Omega) = \frac{R(\Omega)}{R_{\max}(\Omega)} = = \frac{R(\Omega)}{R_{\max}(0^o)}$$ 0 degrees defined as “boresight”

Antenna Gain defined as:

$$G(\Omega) = \frac{4\pi R(\Omega)}{\int_\Omega R(\Omega) \, d\Omega} = \frac{4\pi R(\Omega)}{\Phi}$$

If antenna is isotrophic (same characteristics overall) then $R(\Omega) = R_0$,

$$\Phi_0 = \frac{G_0 \Phi_T}{4\pi}$$

$$\Phi_{RS} = \frac{\Phi_T G_0 A_T}{4\pi R_0^2}$$

$$\frac{\Phi_{\text{Receiver}}}{\Phi_{\text{transmitted}}} = [\frac{G_0}{4\pi R_0^2}][A_T(1-f_A)G_{TS}][\frac{A}{4\pi R_0^2}]$$

Proportional to the transmitted power measured at target

Target properties

Proportional to power received at receiver (satellite)

$$\sigma = A_T (1 - f_A) G_{TS}$$

$$\frac{\Phi_{\text{Receiver}}}{\Phi_{\text{transmitted}}} = \left[\frac{G_0 A}{(4\pi)^2 R_0^4}\right]\sigma$$

& if $G_0 = 4\pi A / \lambda^2$

then

$$\sigma = \frac{\Phi_{\text{transmitted}}}{\Phi_{\text{Receiver}}} \frac{(4\pi)^3 R_0^4}{G_0 \lambda^2}$$

$$\frac{\Phi_{\text{Receiver}}}{\Phi_{\text{transmitted}}} = \frac{\lambda^2}{(4\pi)^3} \int_{Afov} \frac{{G_0}^2 A}{R_0^4} \sigma_0 dA_s$$

$$\frac{\Phi_{\text{Receiver}}}{\Phi_{\text{transmitted}}} = \frac{\lambda^2}{(4\pi)^3 R_0^4} \int_{Afov} A \frac{G(\theta,\phi)^2}{R_0^4} \sigma_0 dA$$

and for a narrow beam: $G(\theta,\phi) = G_0, R_0 \sim \text{constant}$

$$\sigma_0 = \frac{\Phi_{\text{Receiver}}}{\Phi_{\text{transmitted}}} \frac{(4\pi)^3 R_0^4}{G_0^2 \lambda^2 \Delta A}$$

Scattering cross Section, σ_o

(1) Specular Reflection

Near vertical incidence

reflection off mirror-like facets

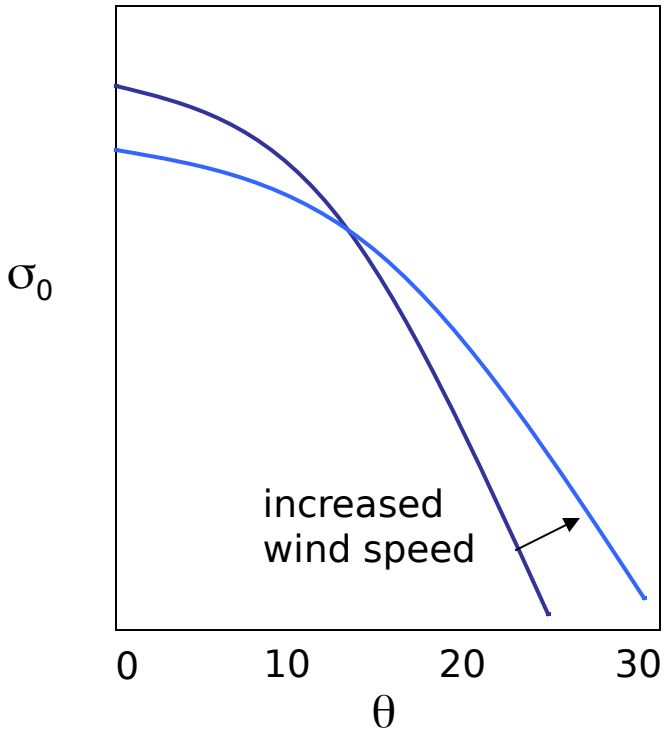

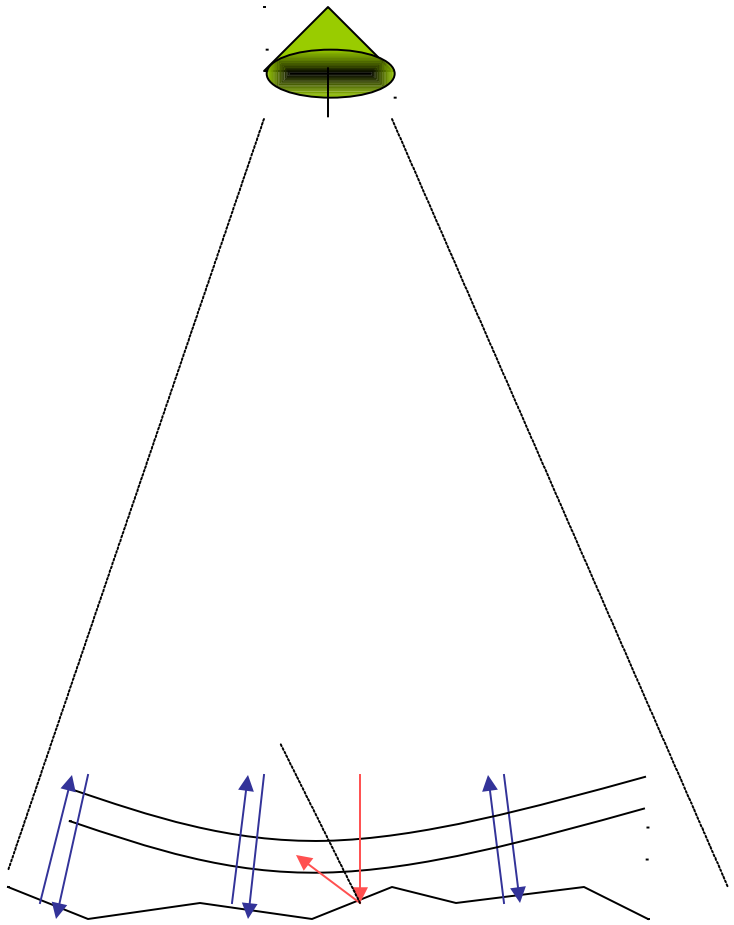

Important for θ < 20° (there are almost no wave slopes > 25°)

σ_0 increases with increasing wind spee
for scatterometer angles

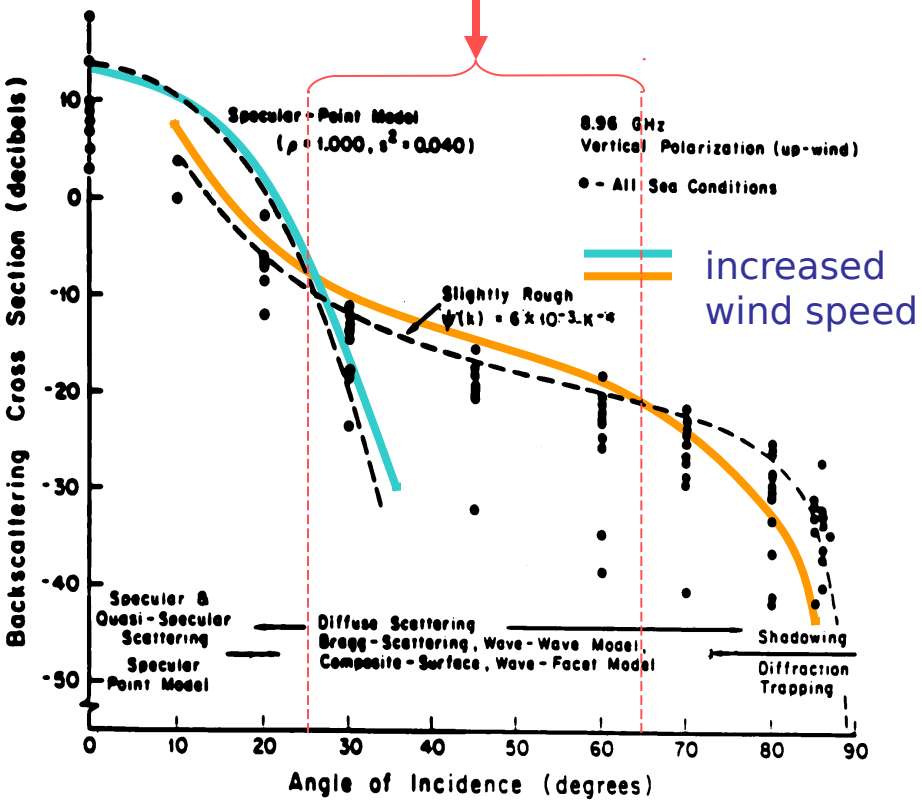

Figure 10.5 Illustration of mechanisms that produce radar backscatter from the ocean at the various angles of incidence (from Valenzuela, 1978).

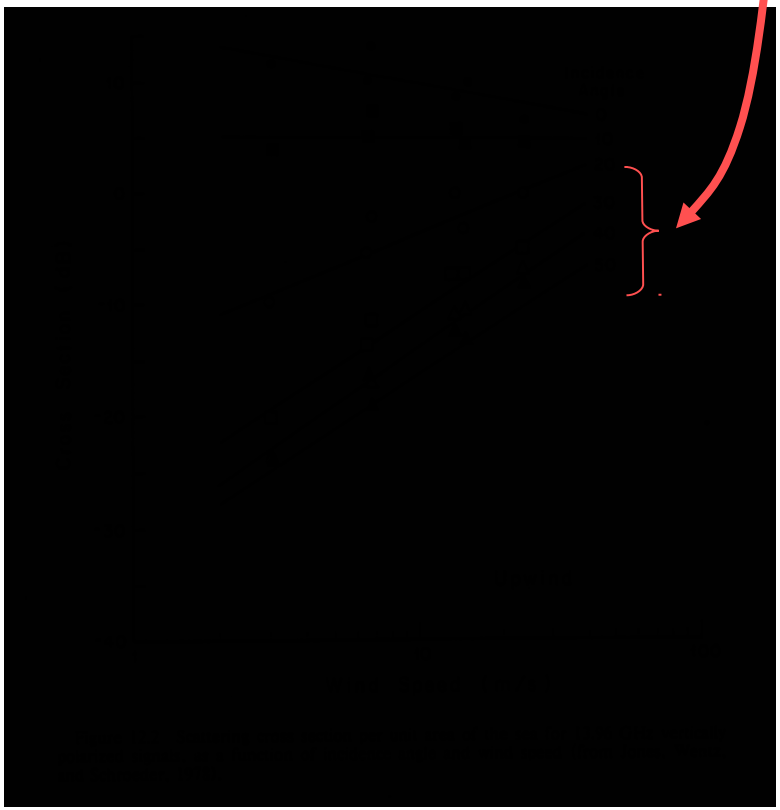

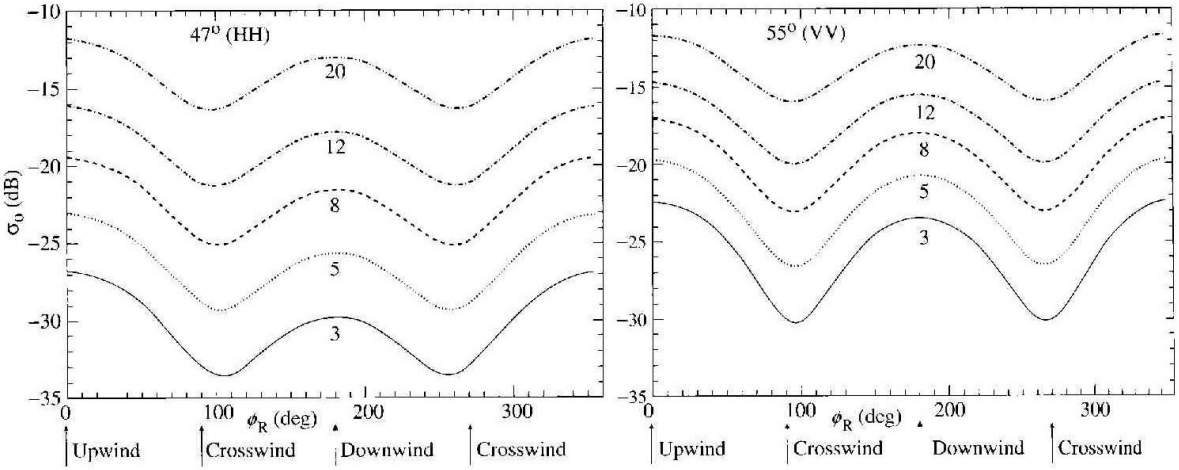

Figure 11.5. The SeaWinds geophysical model function for the SeaWinds incidence angles and polarizations of 47° HH and 55° VV. The curves are lines of constant wind speed; the numbers below each curve give the wind speed in m s^{-1}. Upwind is at 0°; downwind at 180° (Courtesy Michael Freilich, used with permission).

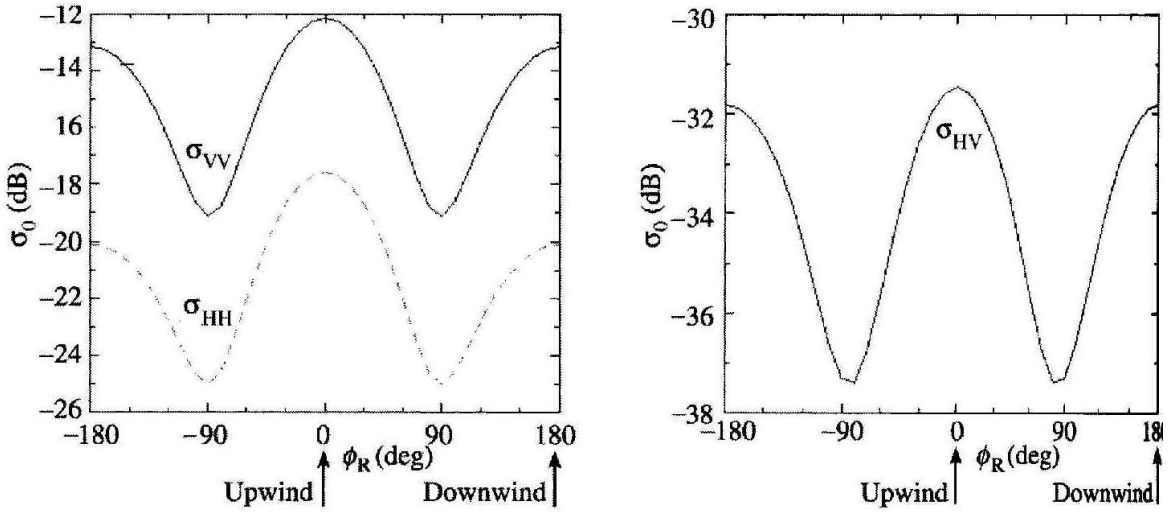

Figure 10.18. Theoretical dependence of σ_0 on ϕ_R for a polarimetric 14 GHz scatterometer at a 45
incidence angle and for a 10 m s^{-1} wind speed (Figure 3 from Yueh *et al.*, 2002, © 2002 IEEE, use
with permission, courtesy Simon Yueh).

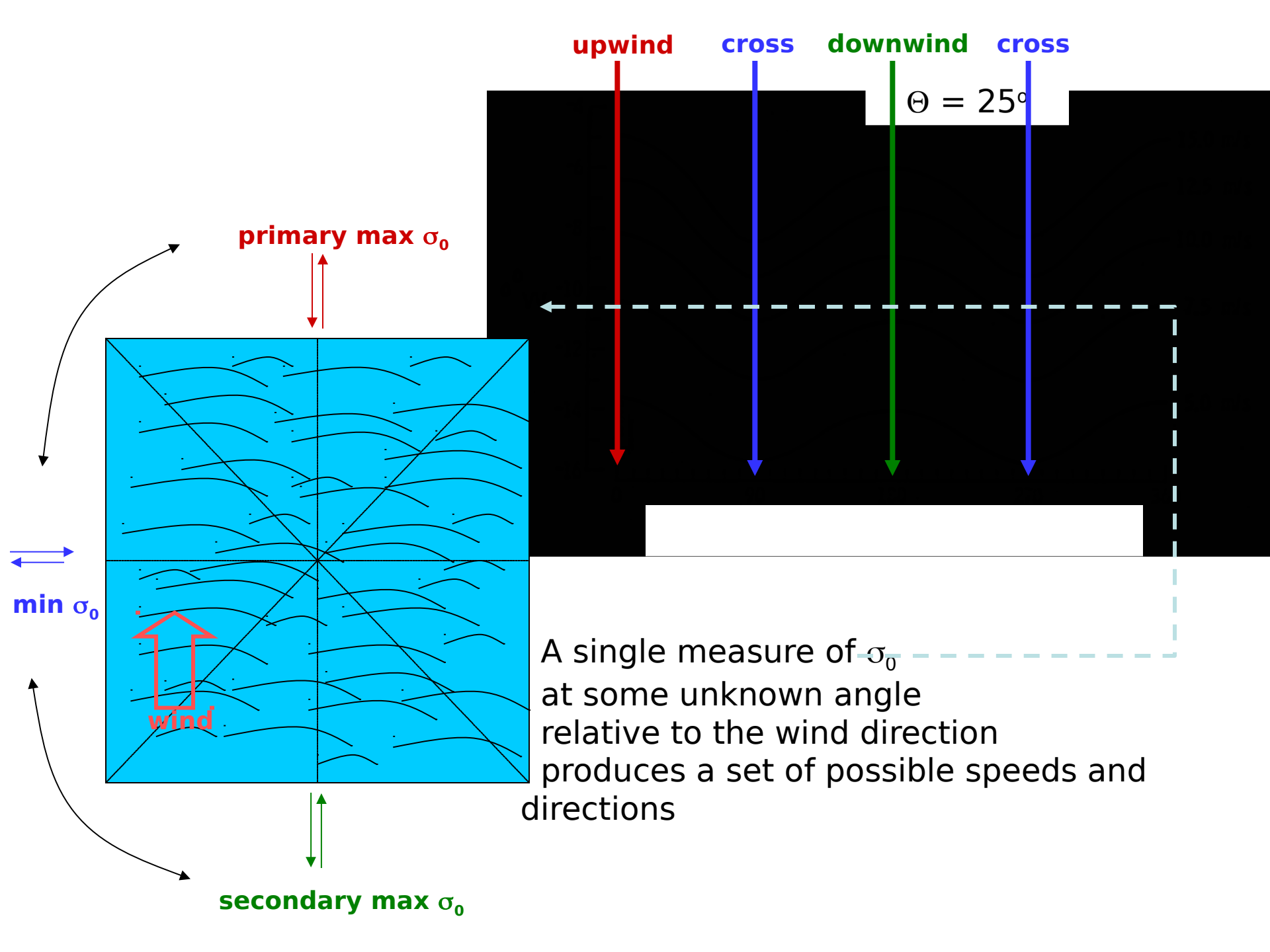

A single measure of σ_0 at some unknown angle relative to the wind direction produces a set of possible speeds and directions

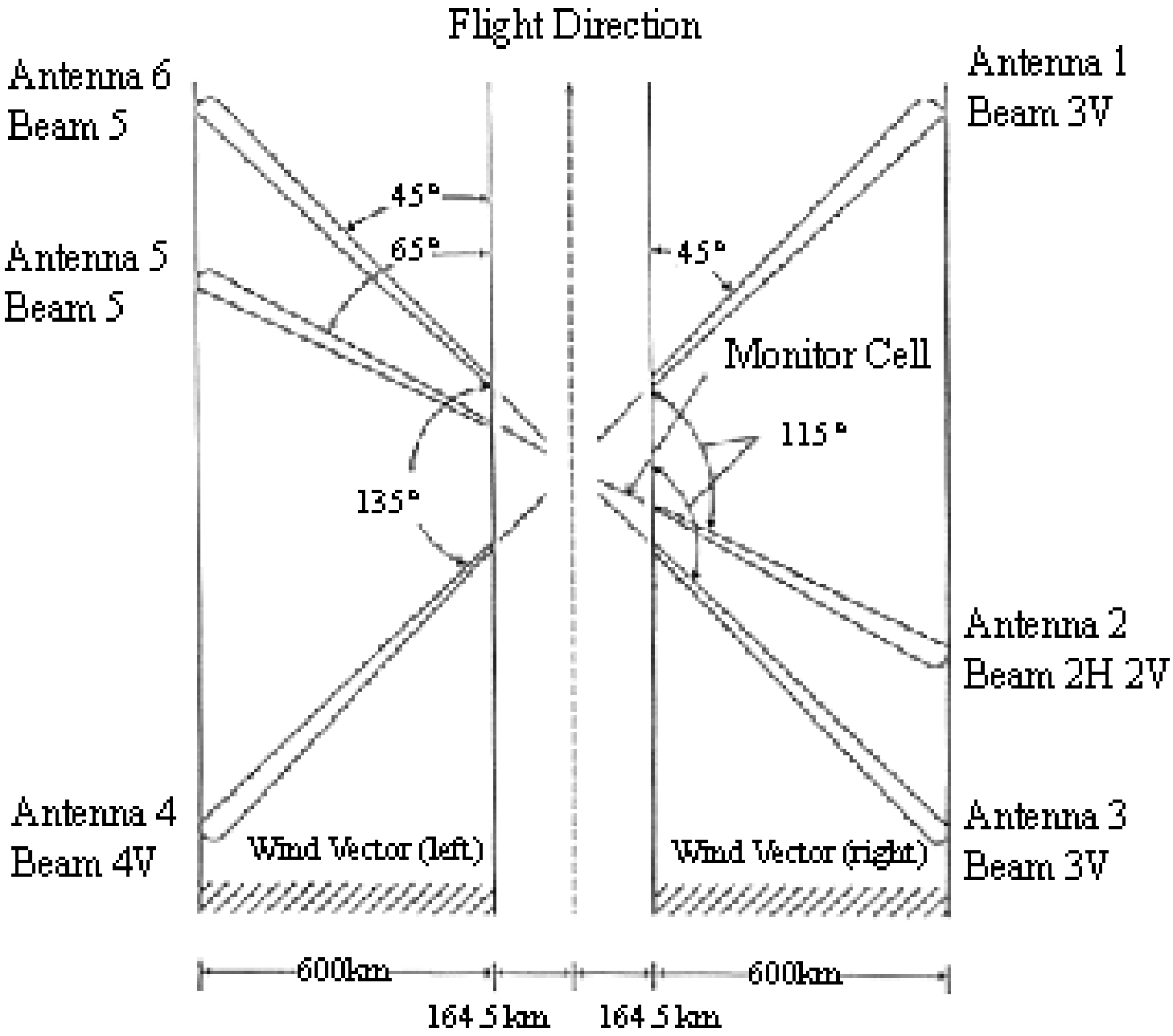
Flight Direction
Antenna 6
Beam 5
Antenna 5
Beam 5
Antenna 1
Beam 3V
45°
65°
45°
Monitor Cell
115°
135°
Antenna 2
Beam 2H 2V
Antenna 4
Beam 4V
Wind Vector (left)
Wind Vector (right)
Antenna 3
Beam 3V
600km
600km
164.5 km
164.5 km

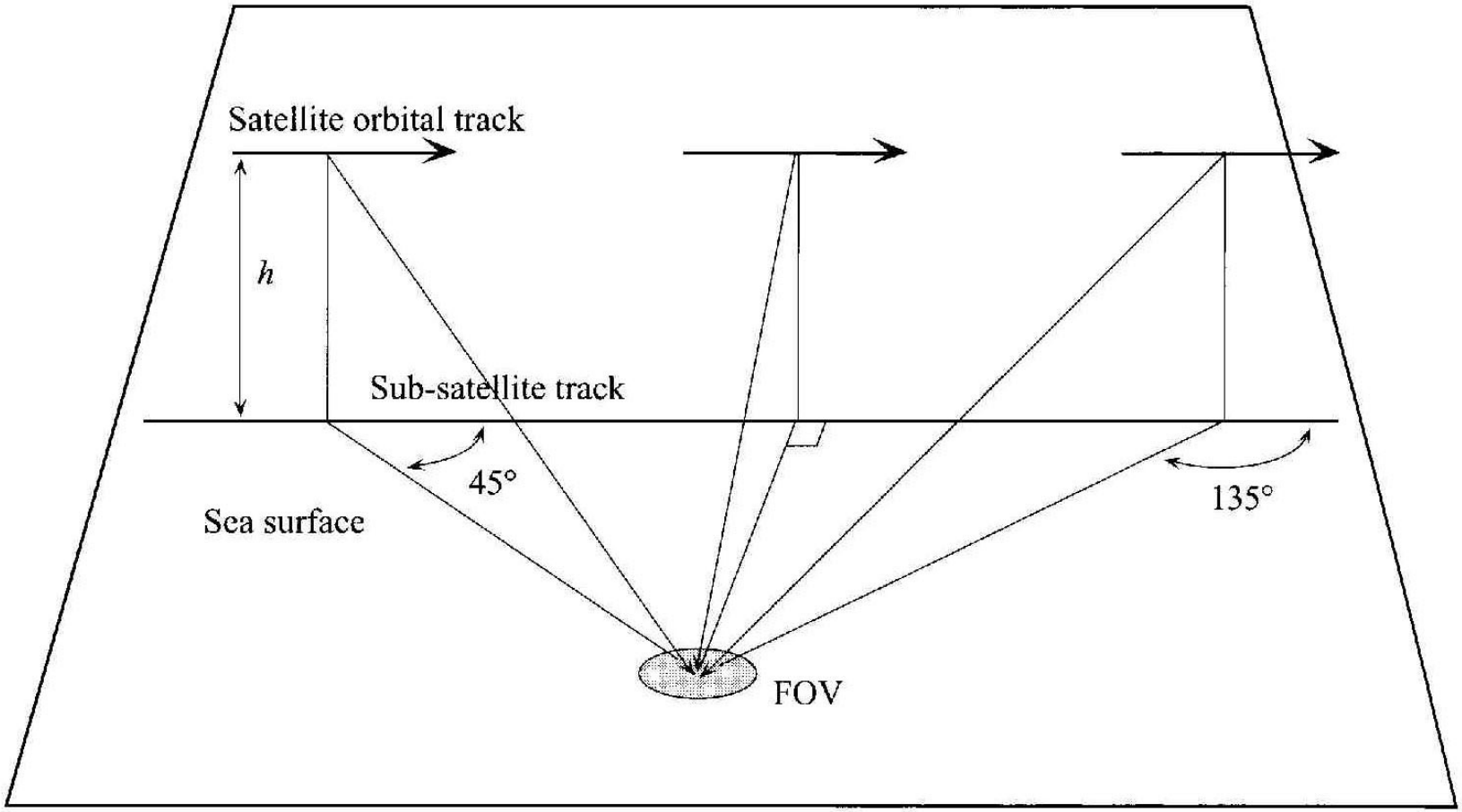

Figure 11.4. Example of several looks by a scatterometer at the same FOV.

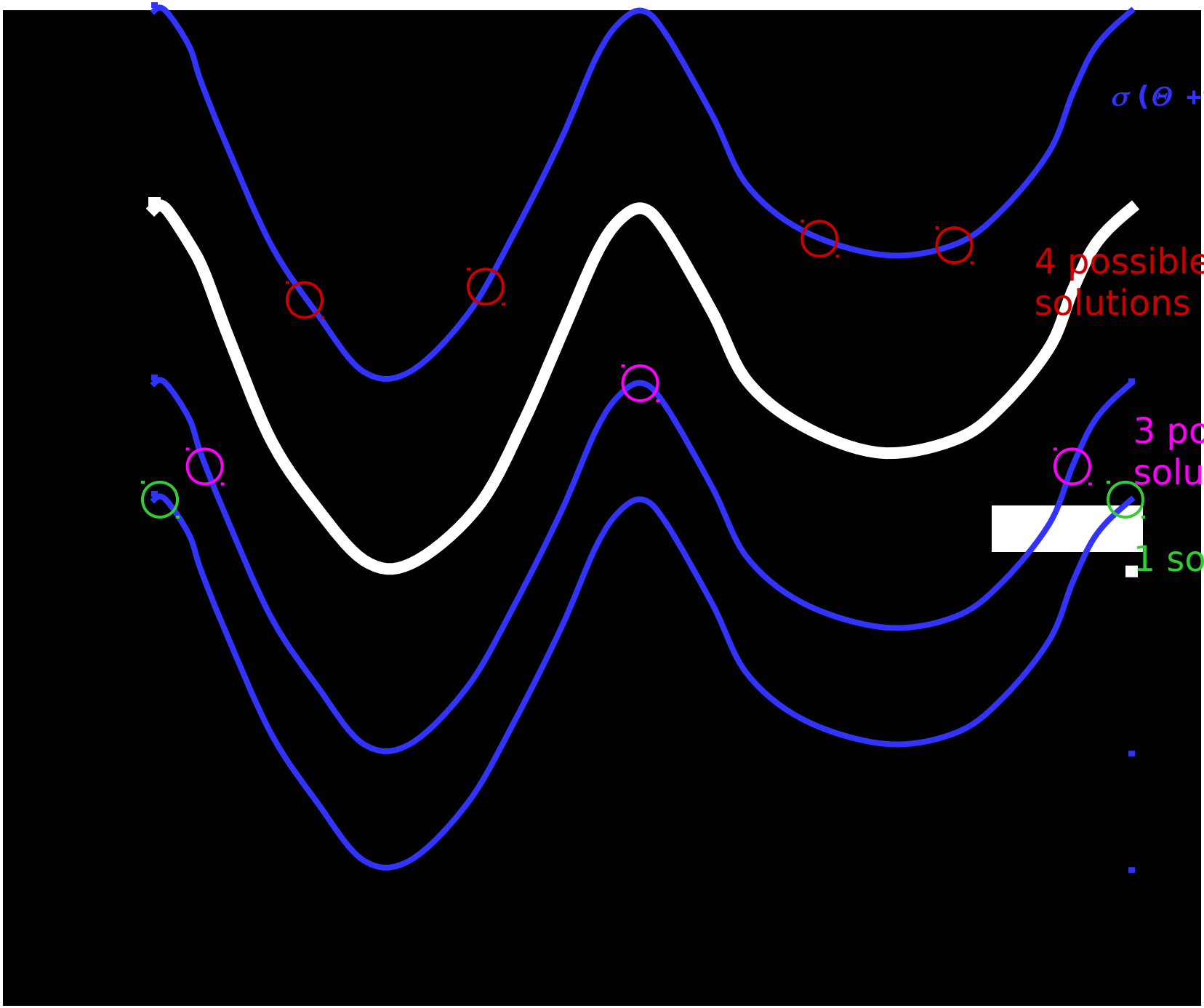
$\sigma(\theta + 90)$
4 possible solutions
3 possible solutions
1 solution

What if a third view direction is added (Θ+20º)

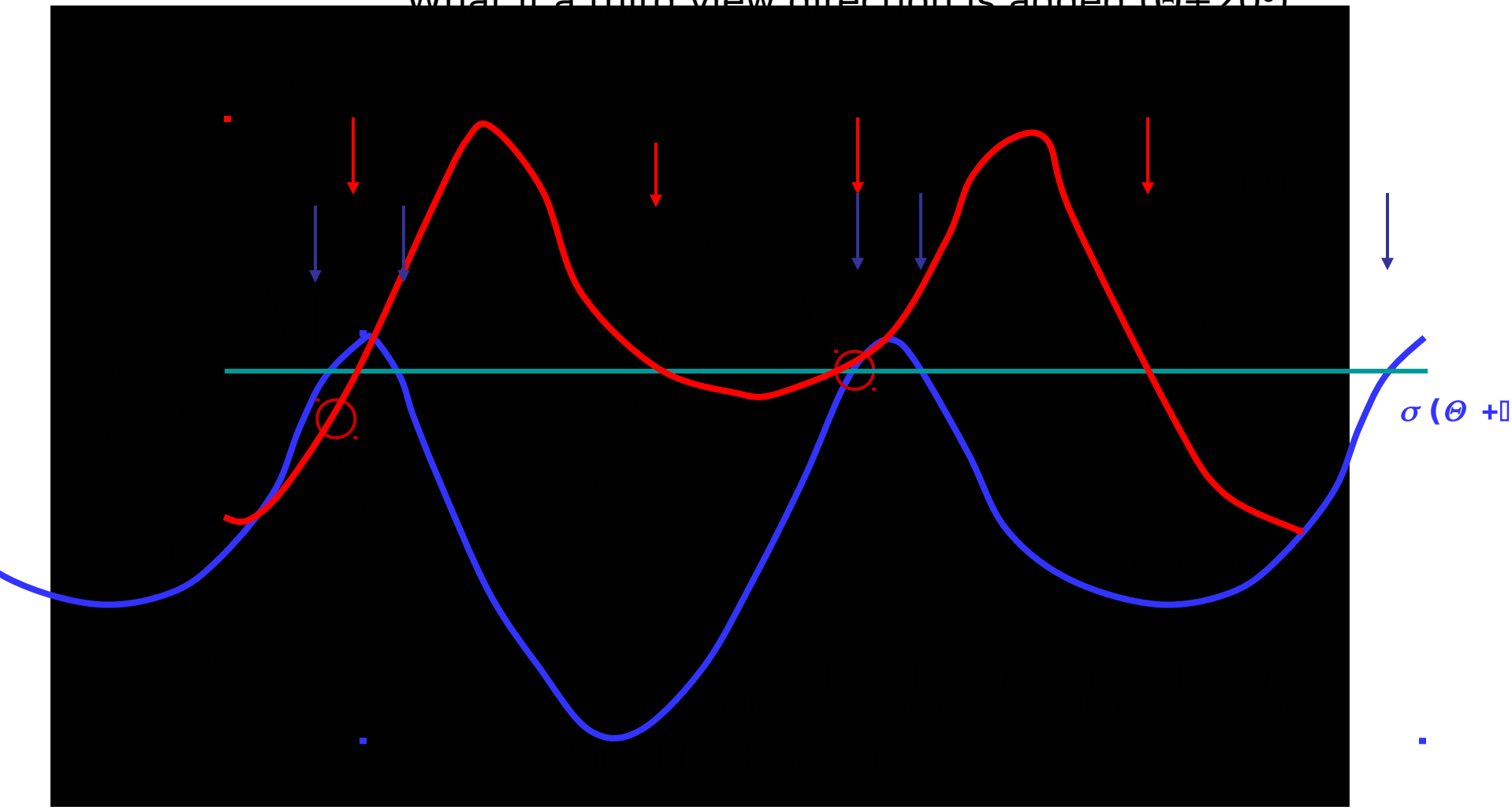

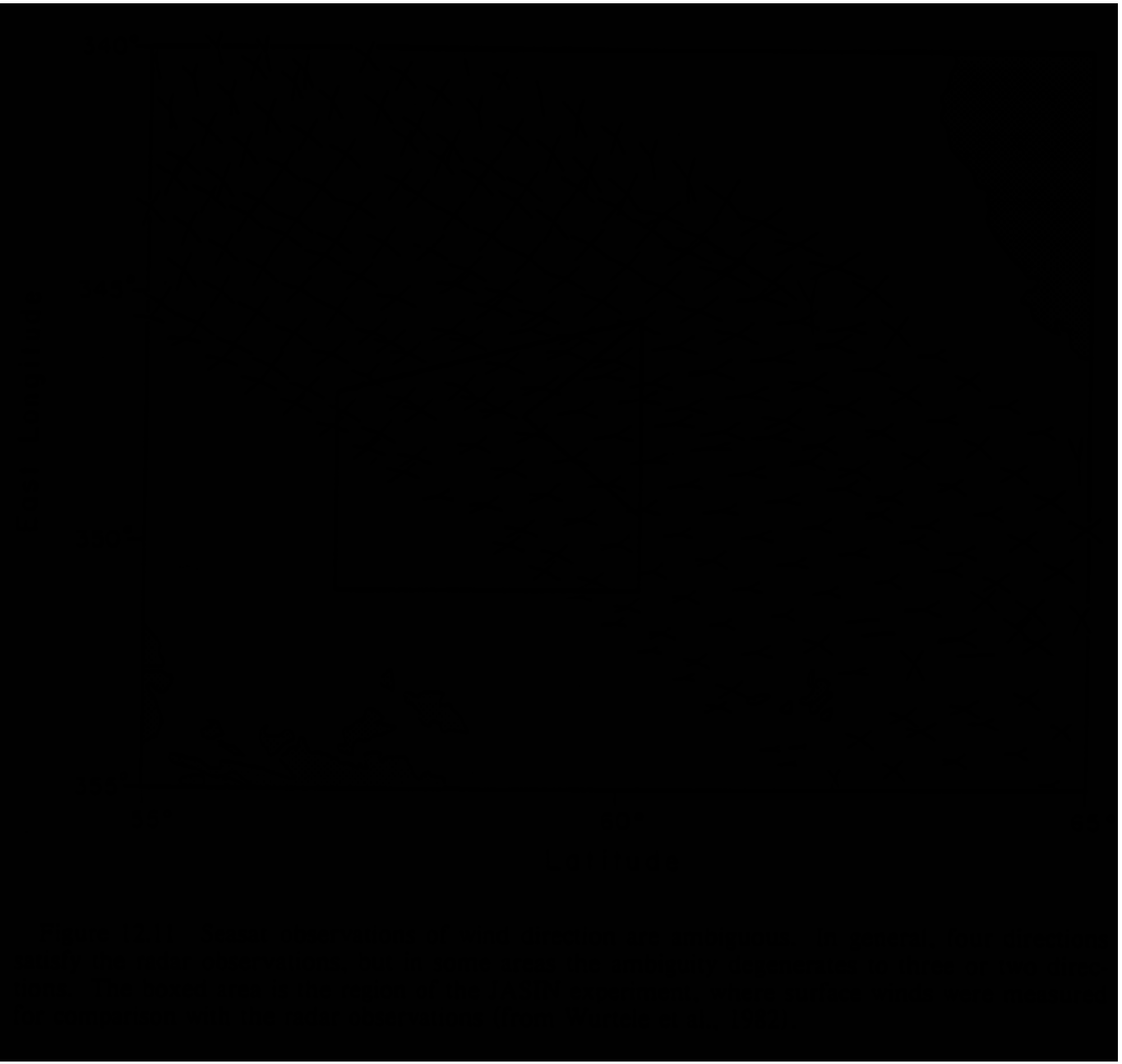

Vector selection:

consistency with the
pressure field

or consistency within
a model analysis
(continuity)

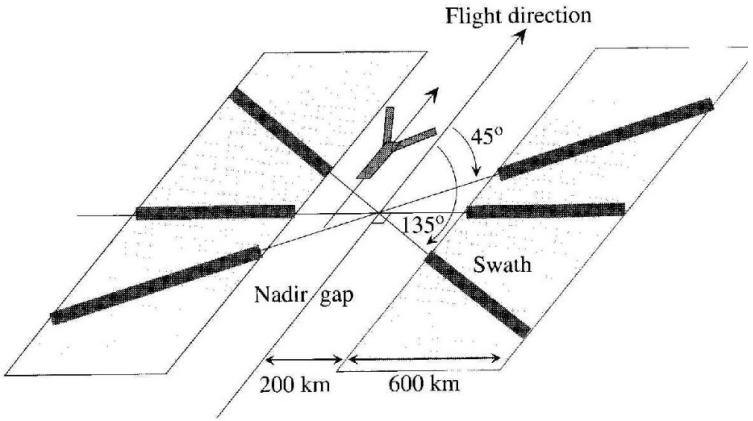

Figure 11.9. The surface swaths of the METOP-1 Advanced Scatterometer (ASCAT) sc launch in 2005 (Adapted from Rostan, 2000).

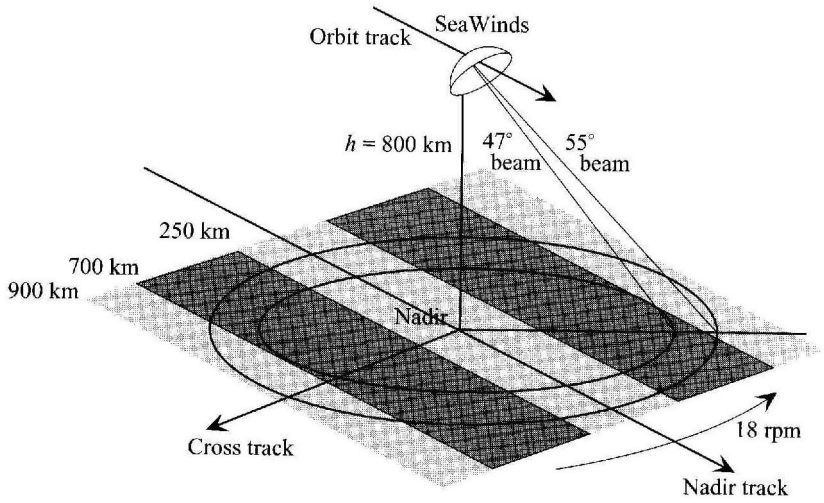

Figure 11.10. The SeaWinds conceptual design and scan coverage for the listed incidence angles. In the dark portion of the swath, the winds are determined from four looks; in the light portion, from two looks (Adapted from an unpublished figure of Michael Freilich).

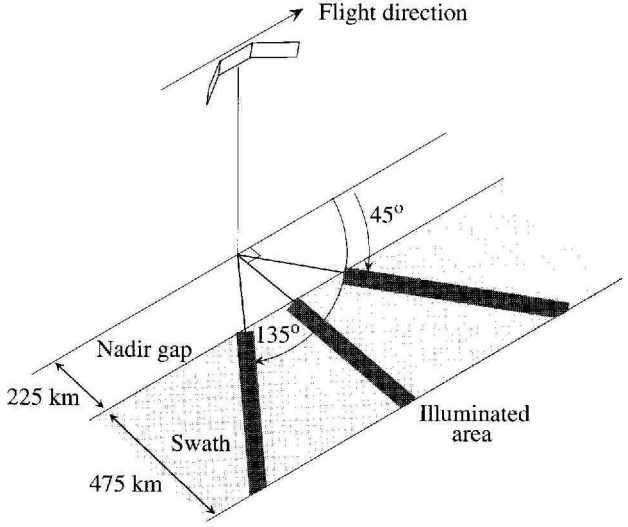

Figure 11.8. The surface swaths of the ERS scatterometer antennas.

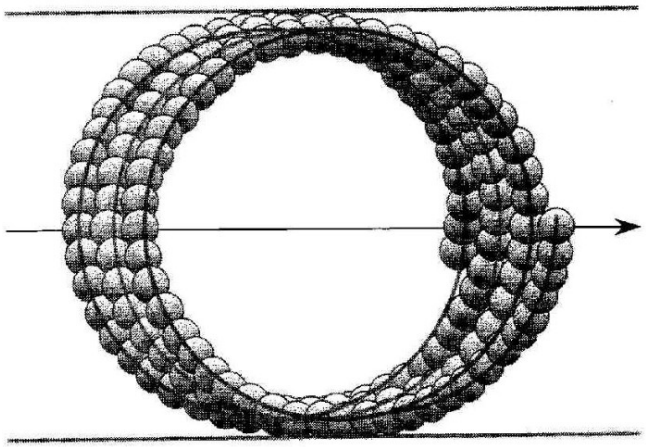

Figure 11.11. The surface scanning pattern of a single SeaWinds beam. The diameter of a single FOV is about 25 km (Figure courtesy Michael Freilich, used with permission).

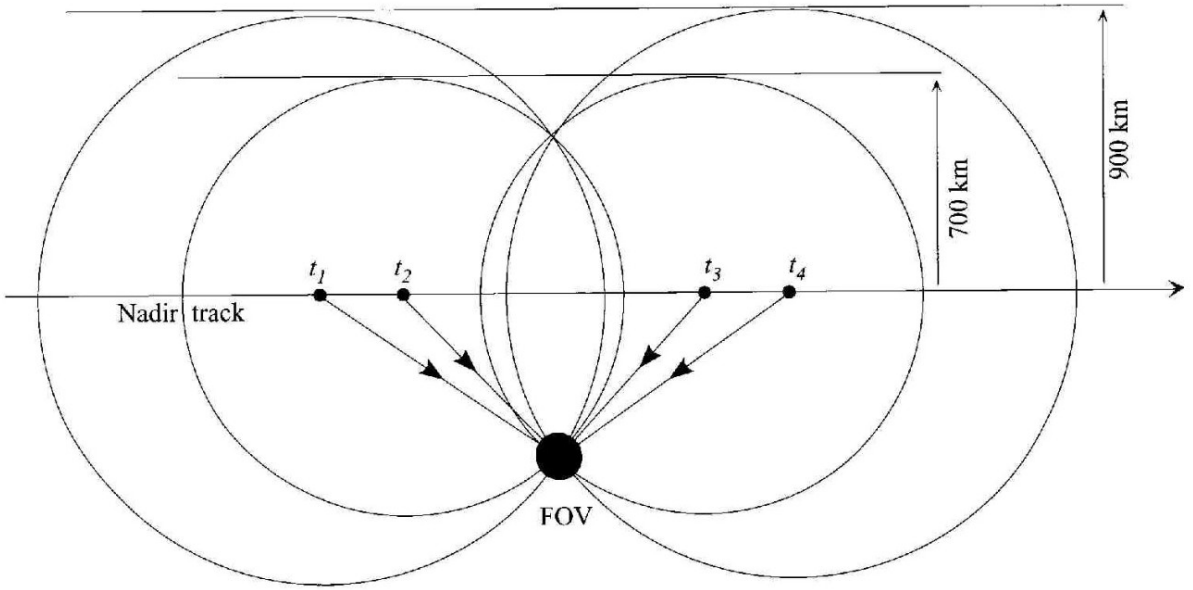

Figure 11.12. An example of how two looks by the outer beam and two looks by the inner beam generate four looks at the same FOV (Redrawn from an undated NASDA publication on ADEOS-2).

Instrument	SASS	AMI (ERS-1, 2)	NSCAT	SeaWinds	ASCAT
Frequency	14.6 GHz	5.3 GHz	13.995 GHz	13.402 GHz	5.3 GHz
Scan pattern	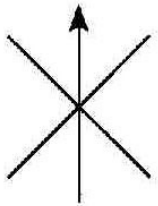	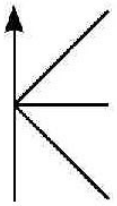	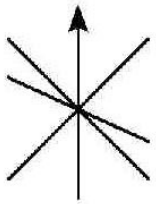	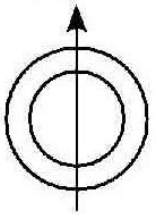	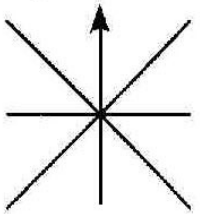
Incidence angle	22°–55°	20°–50°	20°–50°	47°, 55°	20°–50°
Beam resolution	Fixed Doppler	Range binning	Variable Doppler	Scanning pencil	Range binning
Resolution	50 km	50 km	25 km	12.5, 25 km	25 km
Swath	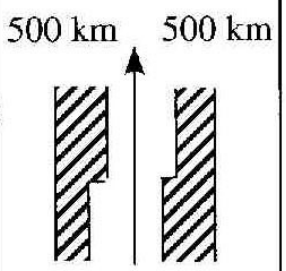	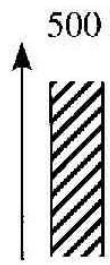	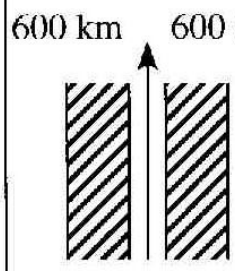	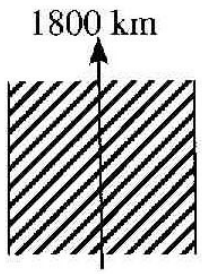	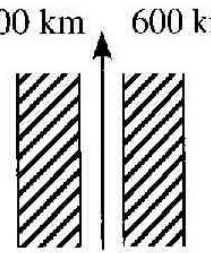
Daily coverage	Variable	41%	77%	93%	80% (estimated)
Operation dates	1978	1991–2001	1996–97	1999–, 2002–03	2005 (estimated)

Figure 11.16. Comparison of the properties of the five scatterometers (Adapted from Figure 3 from Atlas *et al.*, 2001, © 2001 American Meteorological Society, used with permission).

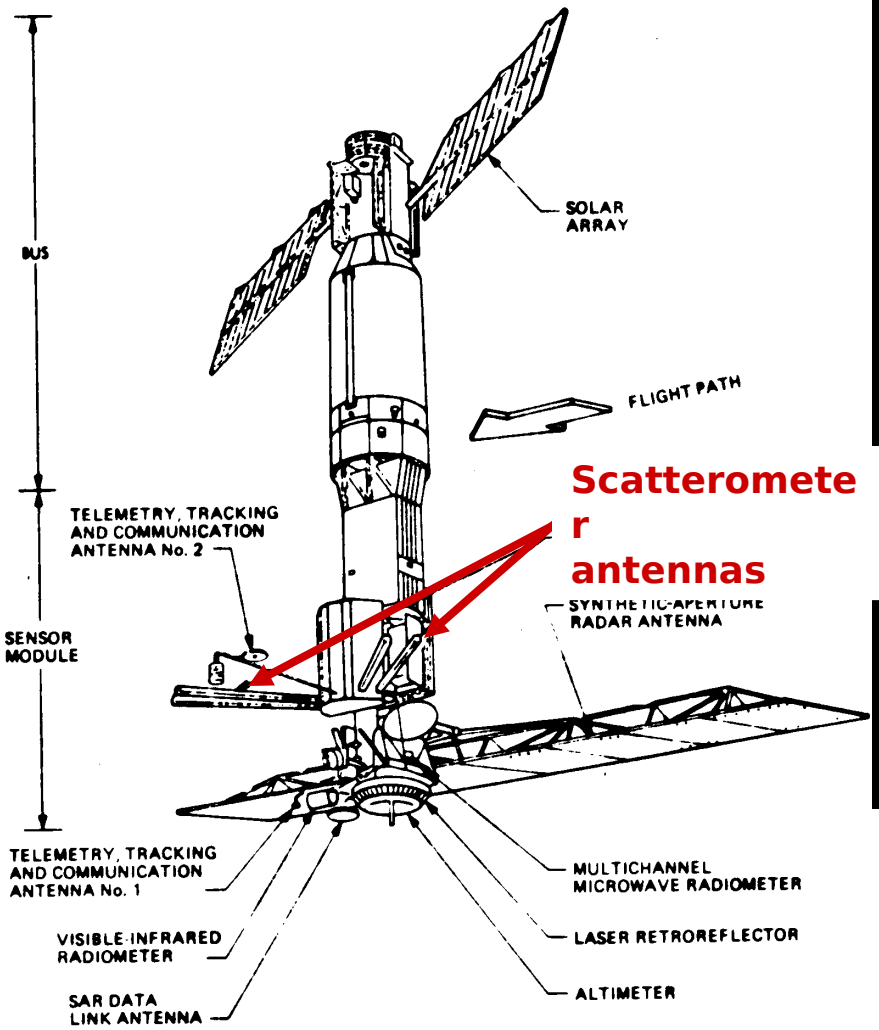

Seasat Scatterometer Pattern

The NASA Scatterometer (NSCAT) was launched on September 15, 1996, measuring global ocean surface wind velocity (both speed and direction). More than 9 months of observations are avail

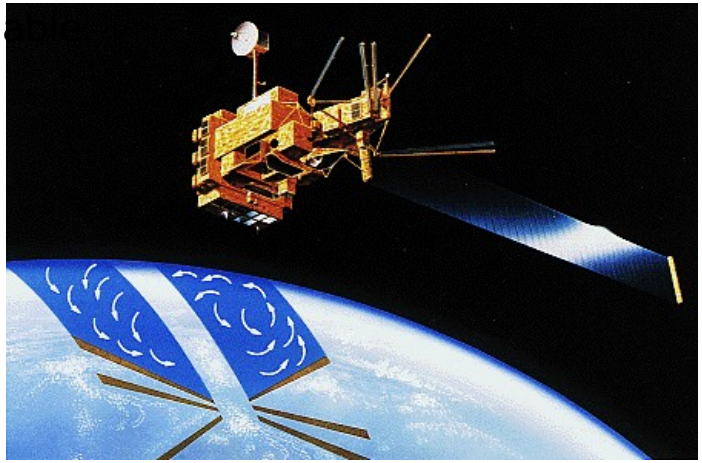

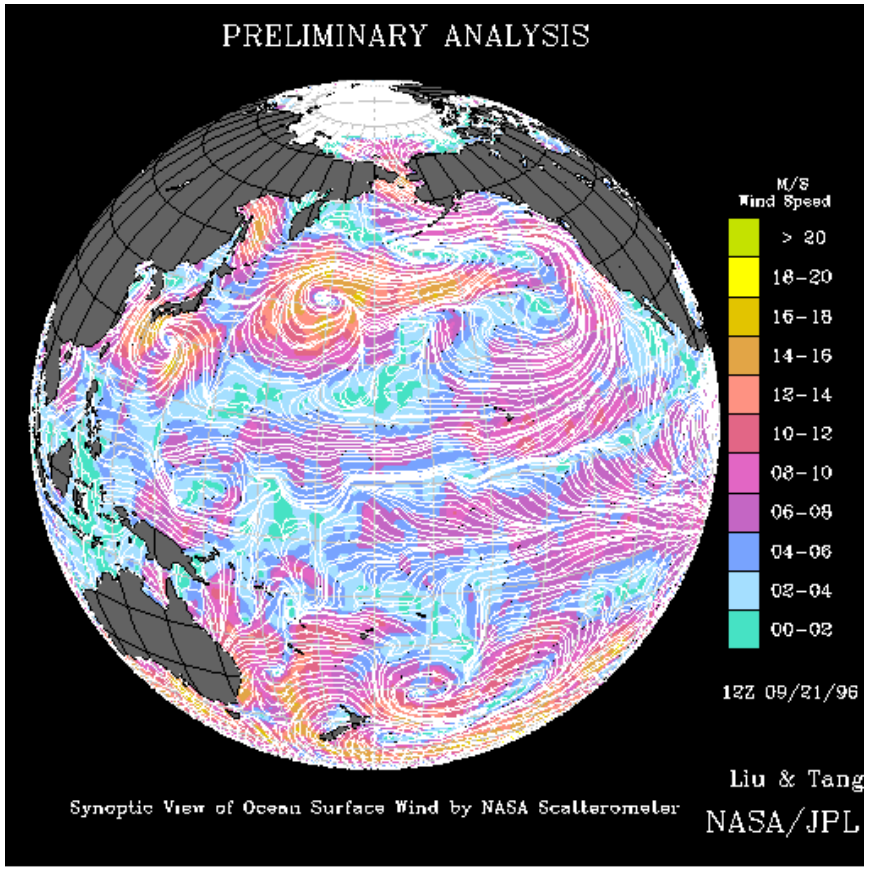

- The instrument was operated continuously at a frequency of 13.995 Giga Hertz.
- Six dual-polarized, 3-meter long, stick-like antennas collected backscatter data with a resolution of 50 km for nine months before loss.
- Backscatter data was combined and processed to yield 268,000 globally distributed wind vectors per day.

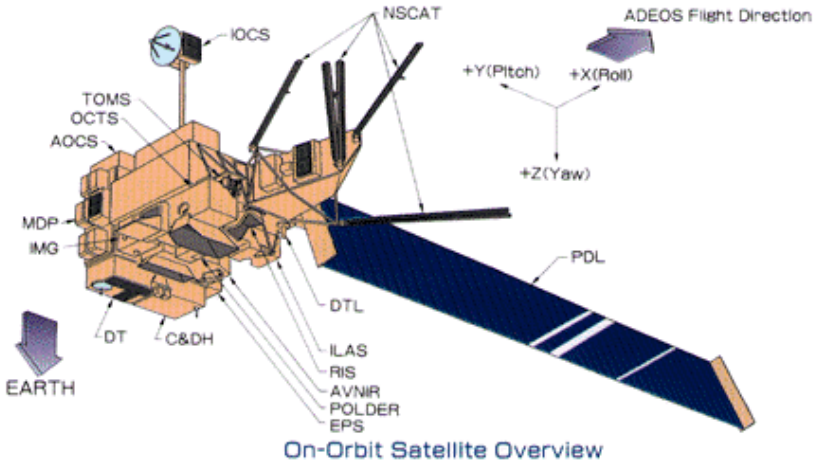

NSCAT Coverage

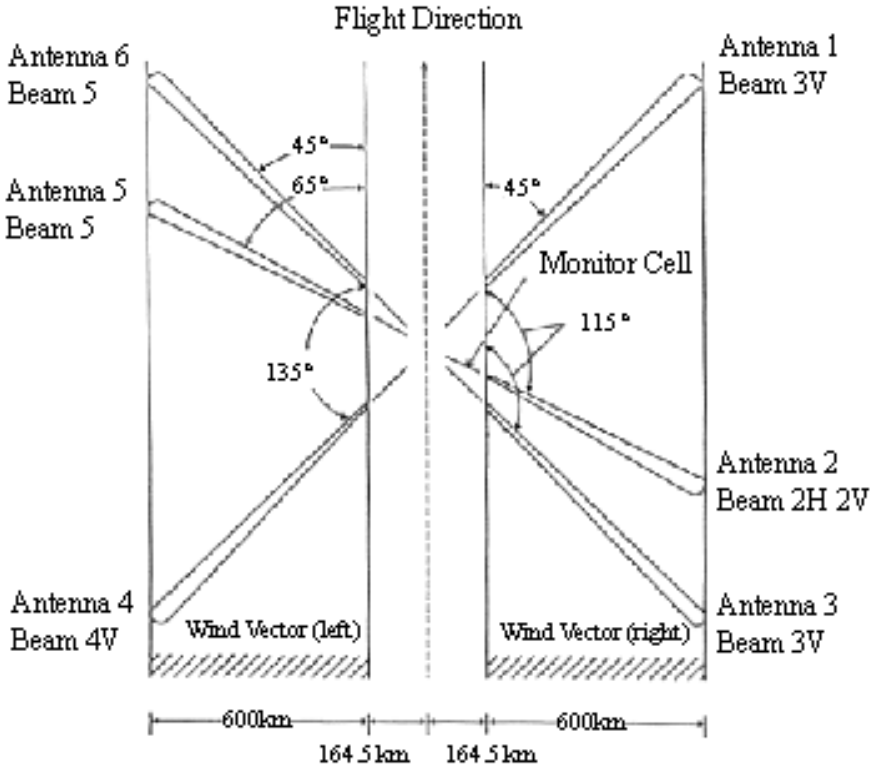

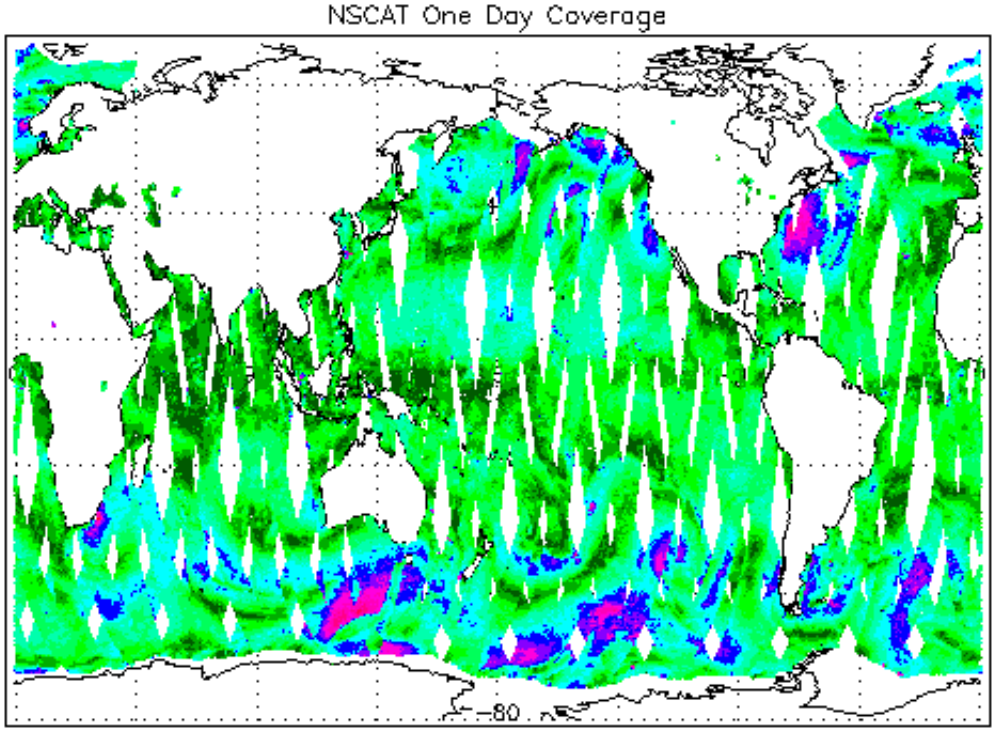

http://manati.wwb.noaa.gov/cgi-bin/qscat_ocean.pl

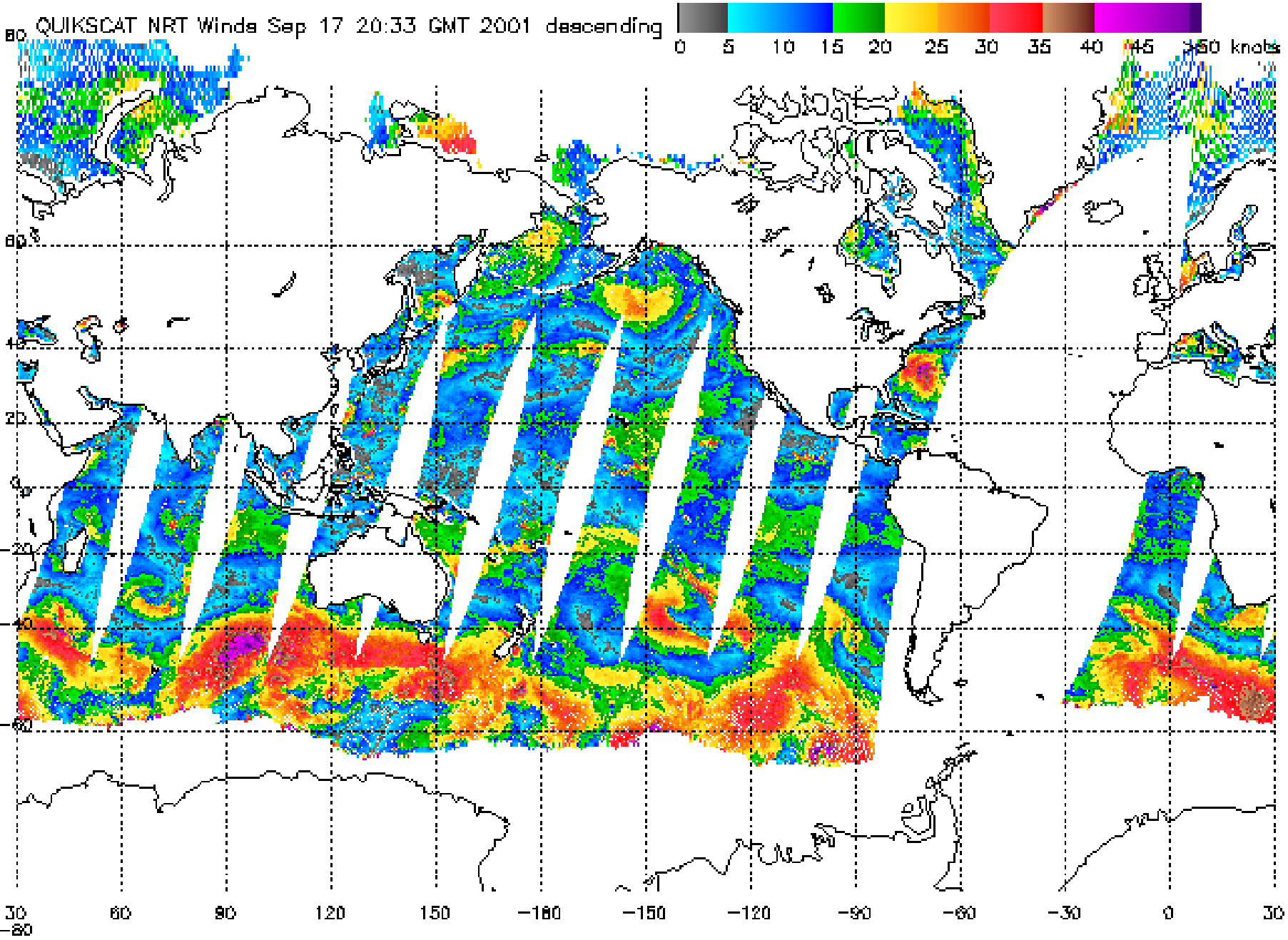

Exploded View of ERS-1

AMI: : Active Microwave Instrument
AOCS : Attitude and Orbital Control System
HPA : High Power Amplifier
IDHT : Instrument Data Handling and Transmission
PDU : Power Distribution Unit

PRARE : Precise Range and Range-rate Equipment
SAR : Synthetic Aperture Radar
RF : Radio Frequency
OBDH : On Board Data Handling
LBR: : Low Bit Rate

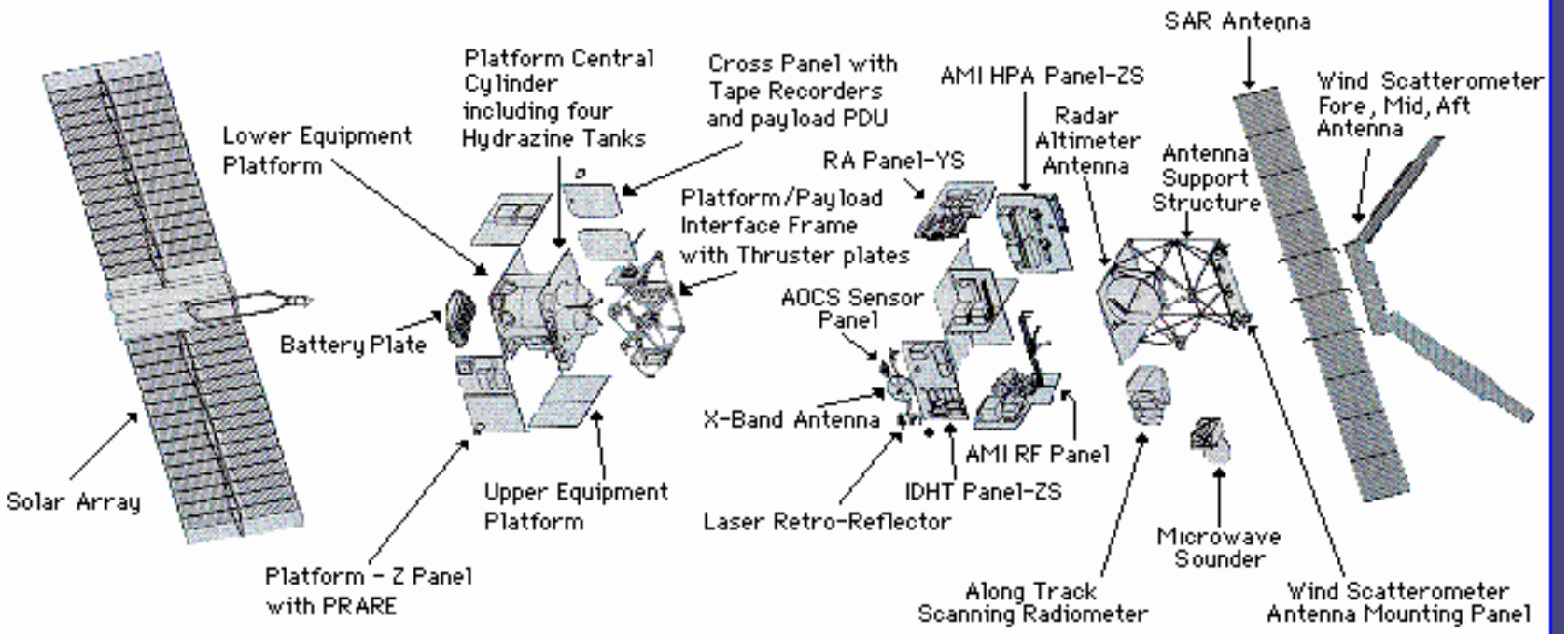

Exploded view of ERS-1 and summary technical specifications

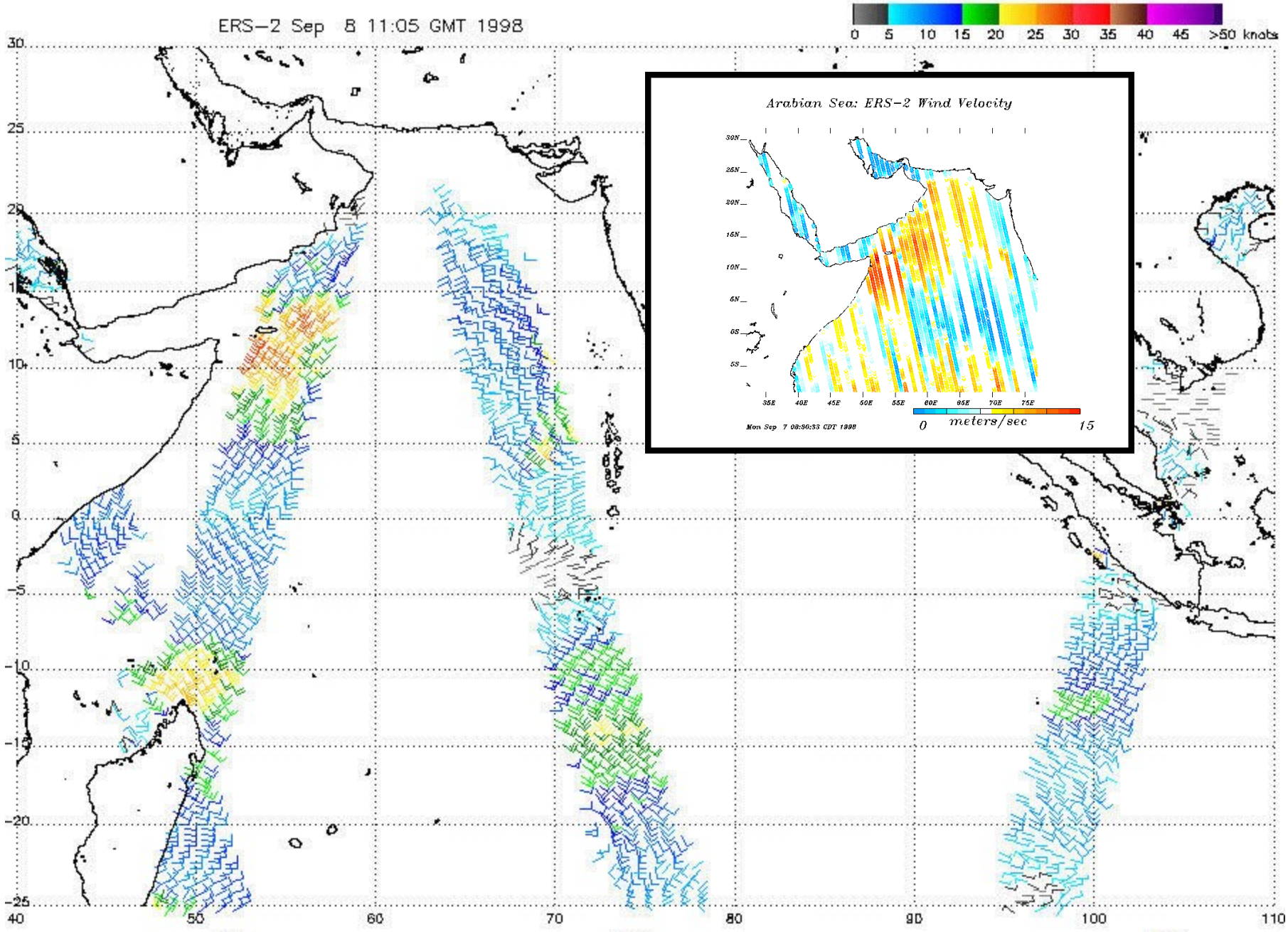

Note: 1) Times are GMT 2)Times correspond to 10S; right swath edge – time is right swath for overlapping swaths at 10S 3) Sep 8 11:05 GMT 1998–18 hrs

NOAA/NESDIS/Office of Research and Applications

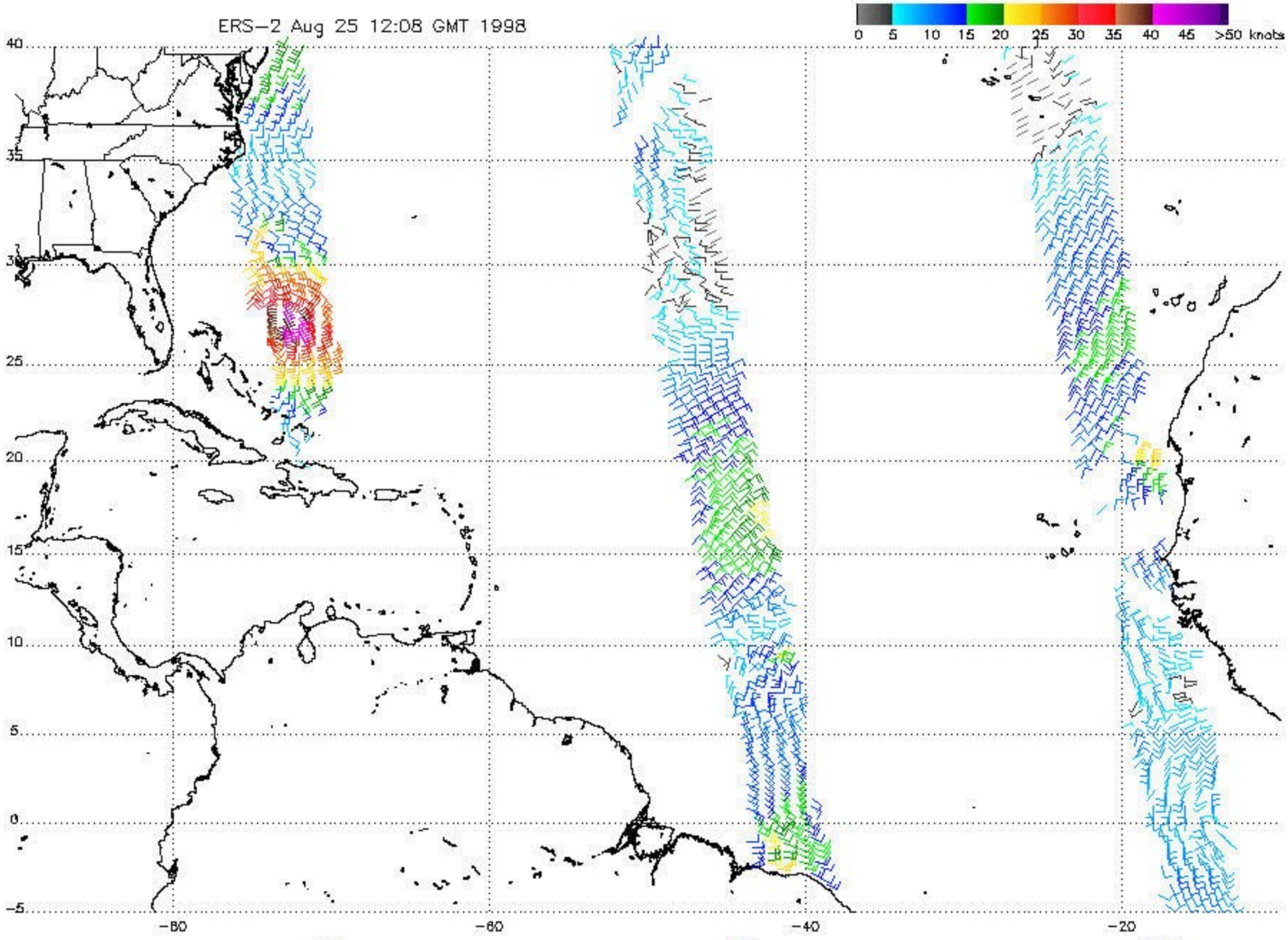

Note: 1) Times are GMT 2)Times correspond to 25N; right swath edge – time is right swath for overlapping swaths at 25N 3) Aug 25 12:08 GMT 1998–16 hrs

NOAA/NESDIS/Office of Research and Applications

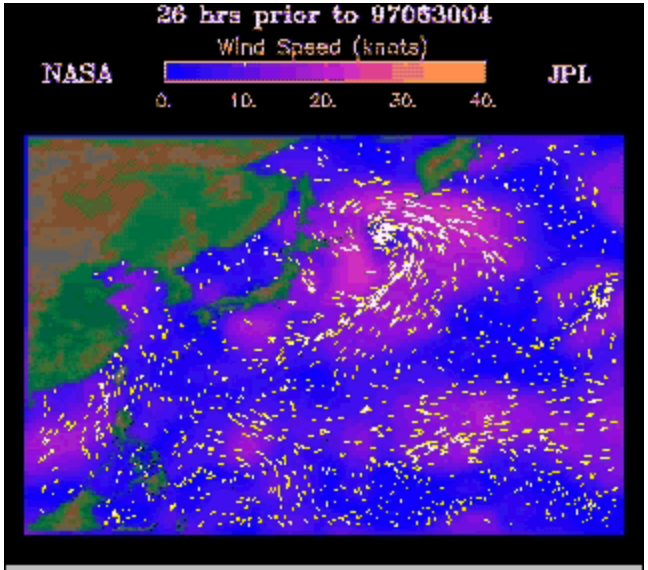

daily_nwpac

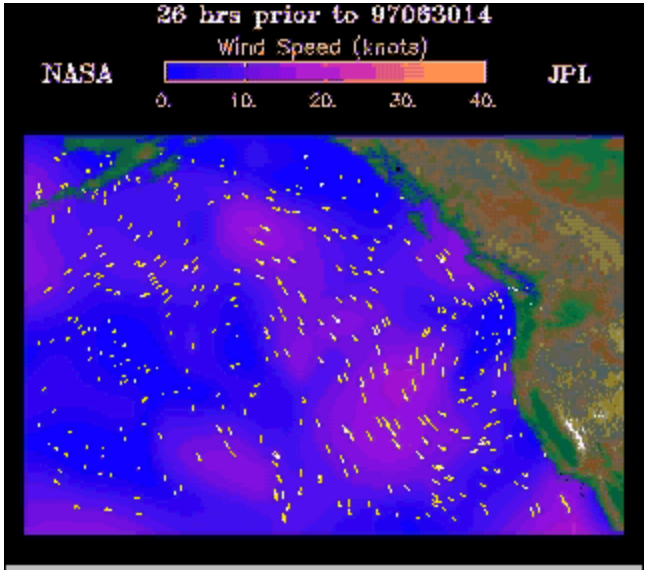

daily_nepac

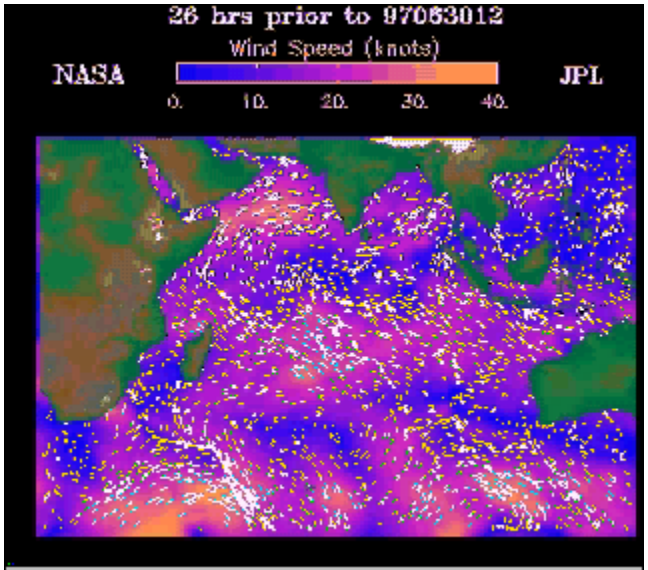

daily_indian

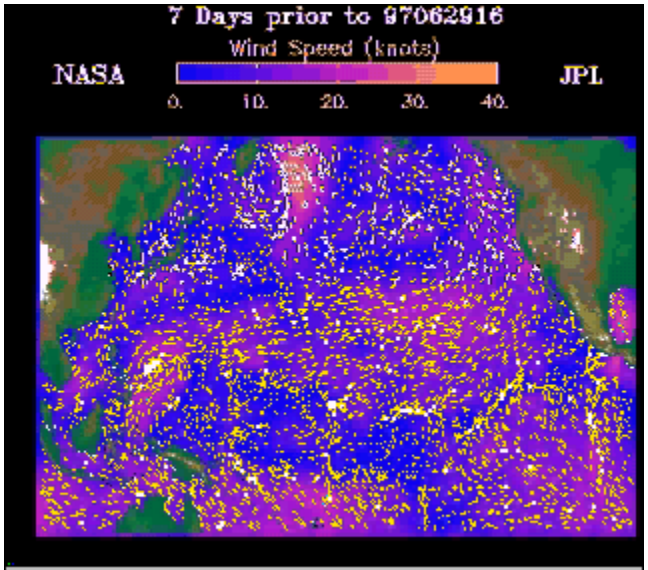

daily_npac_evol

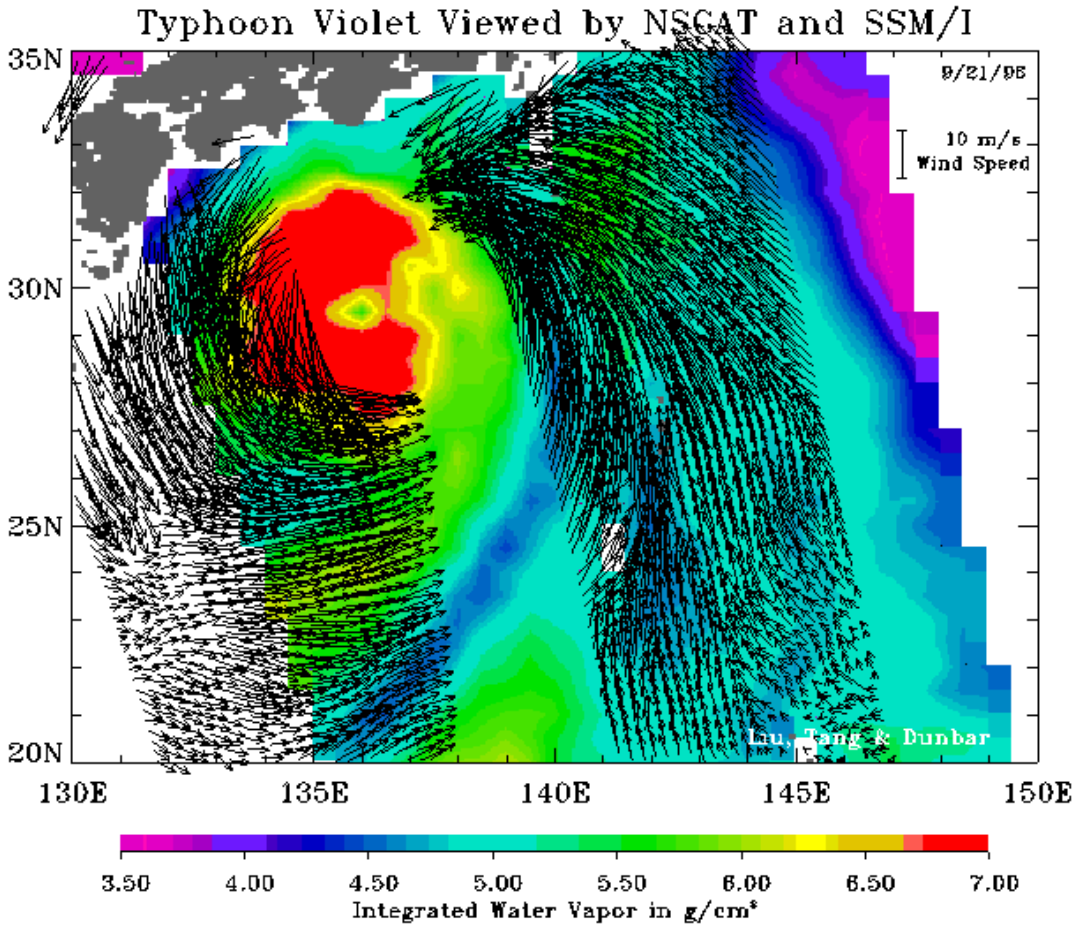
Typhoon Violet Viewed by NSCAT and SSM/I
9/21/96
10 m/s
Wind Speed
35N
30N
25N
20N
130E
135E
140E
145E
150E
Liu, Tang & Dunbar
3.50
4.00
4.50
5.00
5.50
6.00
6.50
7.00
Integrated Water Vapor in g/cm²

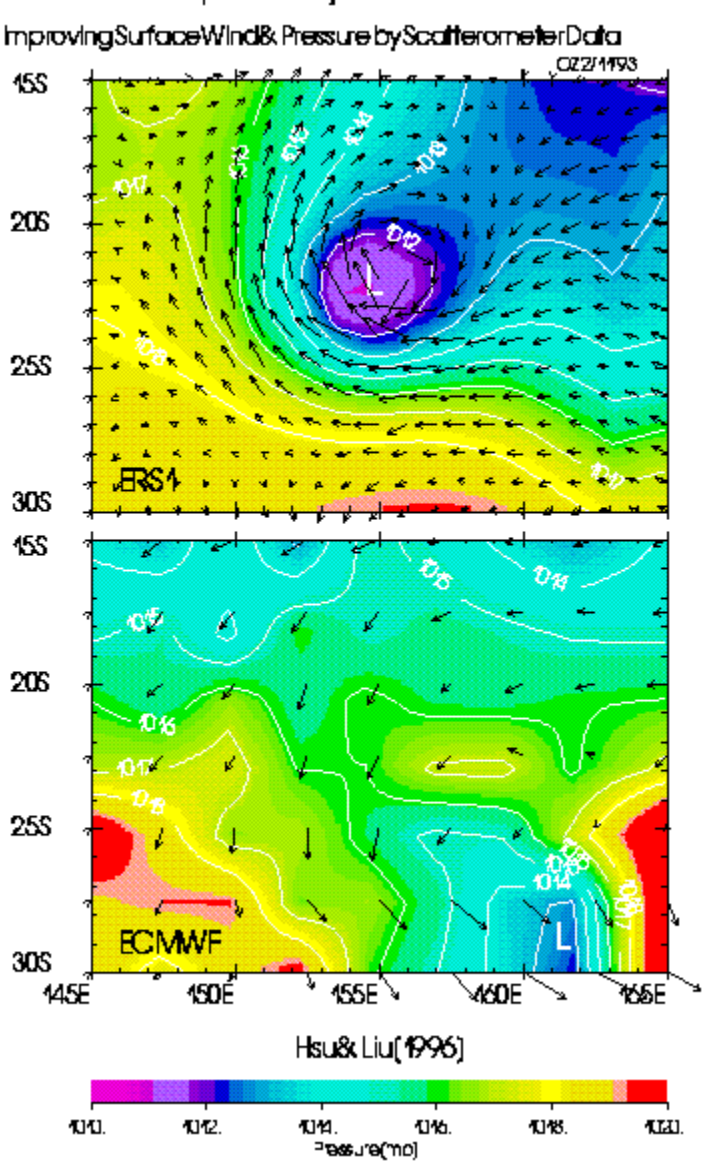
Tropical Cyclone Oliver
Improving Surface Wind & Pressure by Scatterometer Data
OCT/1993
15S
20S
25S
30S
ERS1
ECMWF
L
145E
150E
155E
160E
165E
Hsu & Liu (1996)
1010.
1012.
1014.
1016.
1018.
1020.
Pressure (mb)

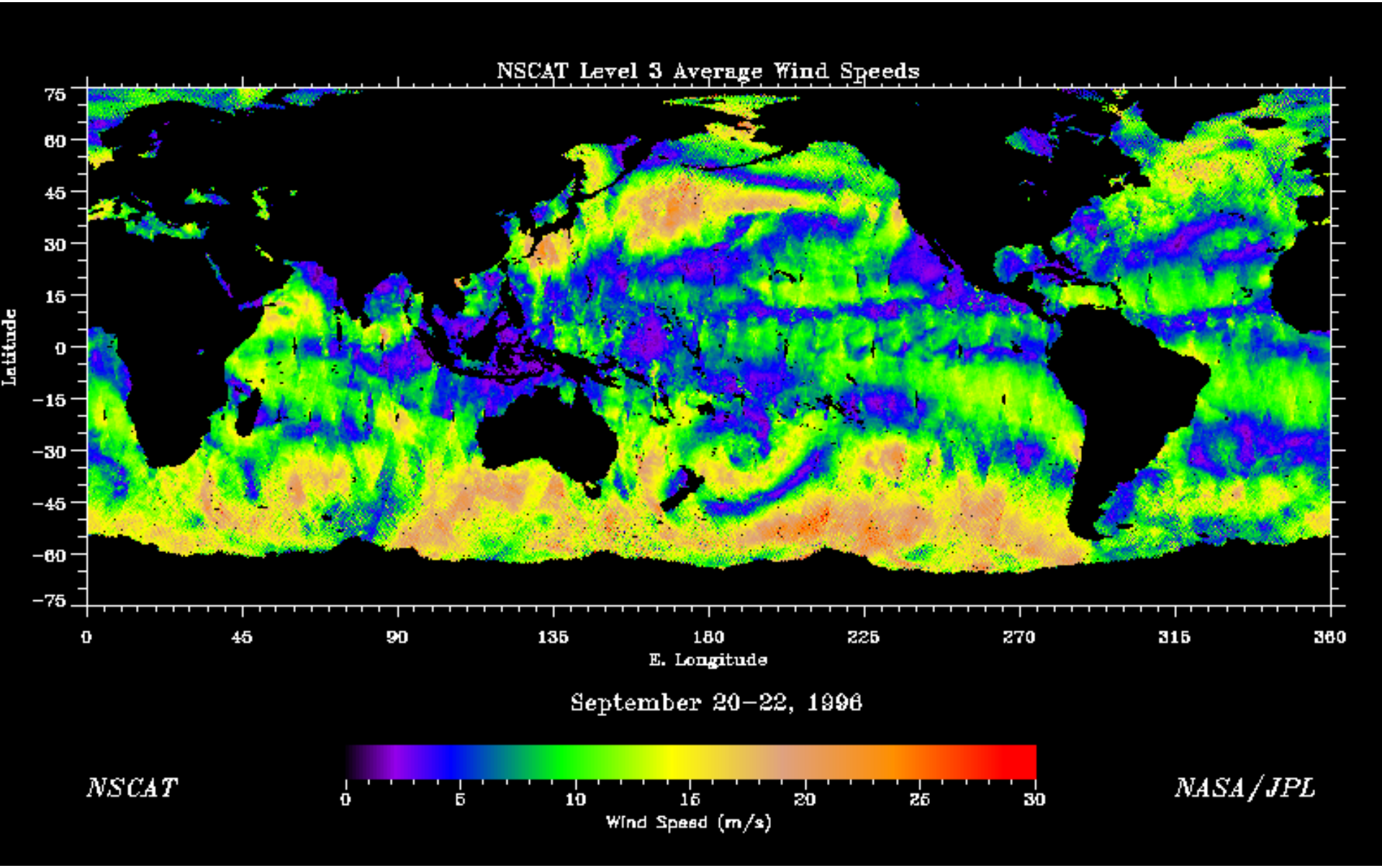

http://www.eorc.nasda.go.jp/ADEOS/FirstImages/images/P47491.gif

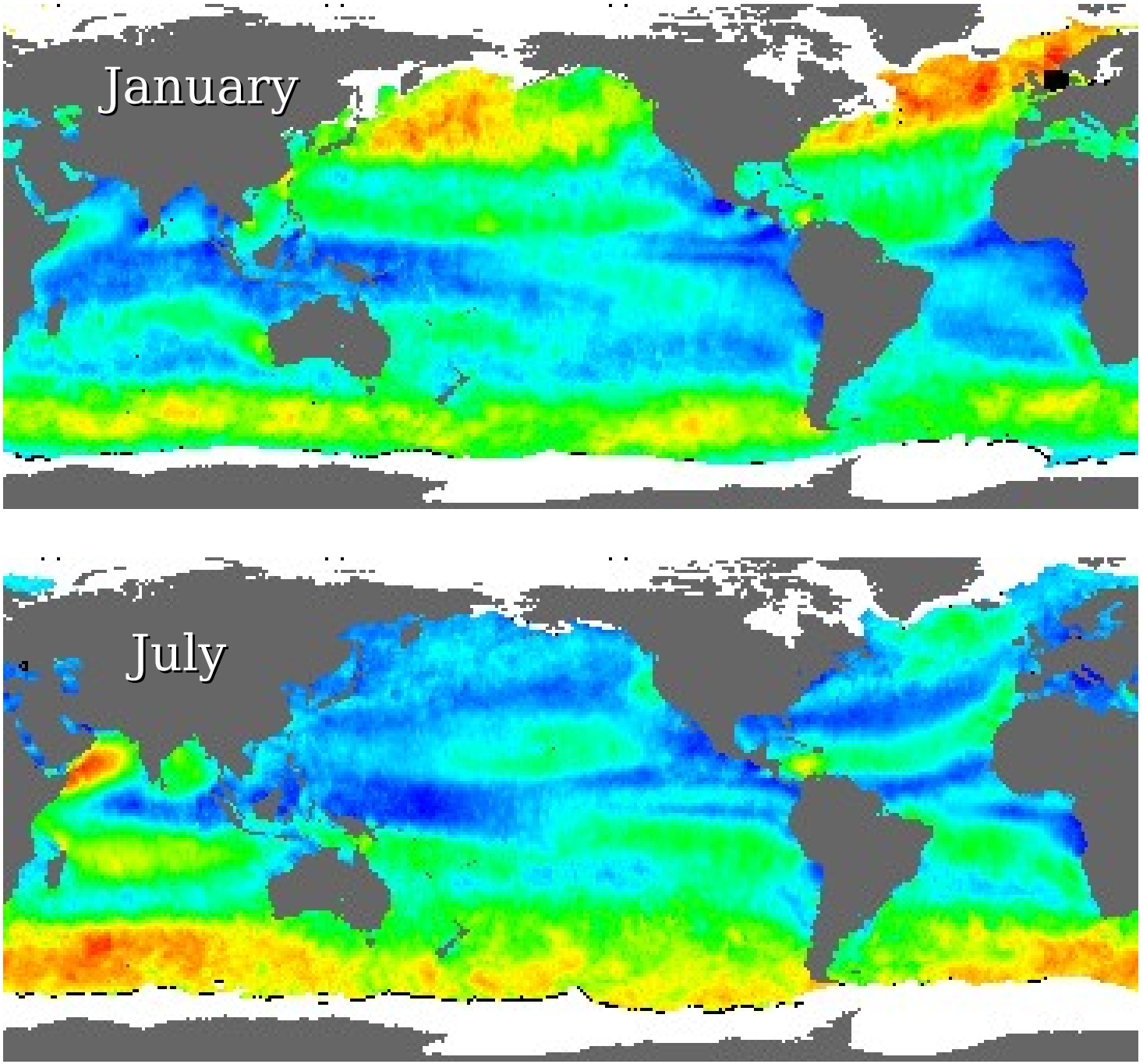
January
July

APPLICATIONS

Weather Forecasting

- Data from ocean scatterometers greatly enhances overall weather-forecasting capabilities.

Storm Detection

- The ocean scatterometer data can determine the location, direction, structure and strength of storms at sea.

Ship Routing

- Wind-observation data from ocean scatterometers is of particular significance in ship routing.

Oil Production

- Earth's oceans are increasingly used as a source of fuel. Thorough knowledge of the historical wind and wave conditions at any specific location is crucial to the design of drilling platforms.
- In the event of an oil spill, surface-wind information is key to determining how the oil will spread.

Food Production

- Perhaps the oldest use of the ocean is in the harvesting of food. The annual U.S. shrimp harvest in the Gulf of Mexico, for example, depends on favorable on-shore winds that transport offshore, plankton larvae to estuaries where the larvae can develop into adult shrimp.

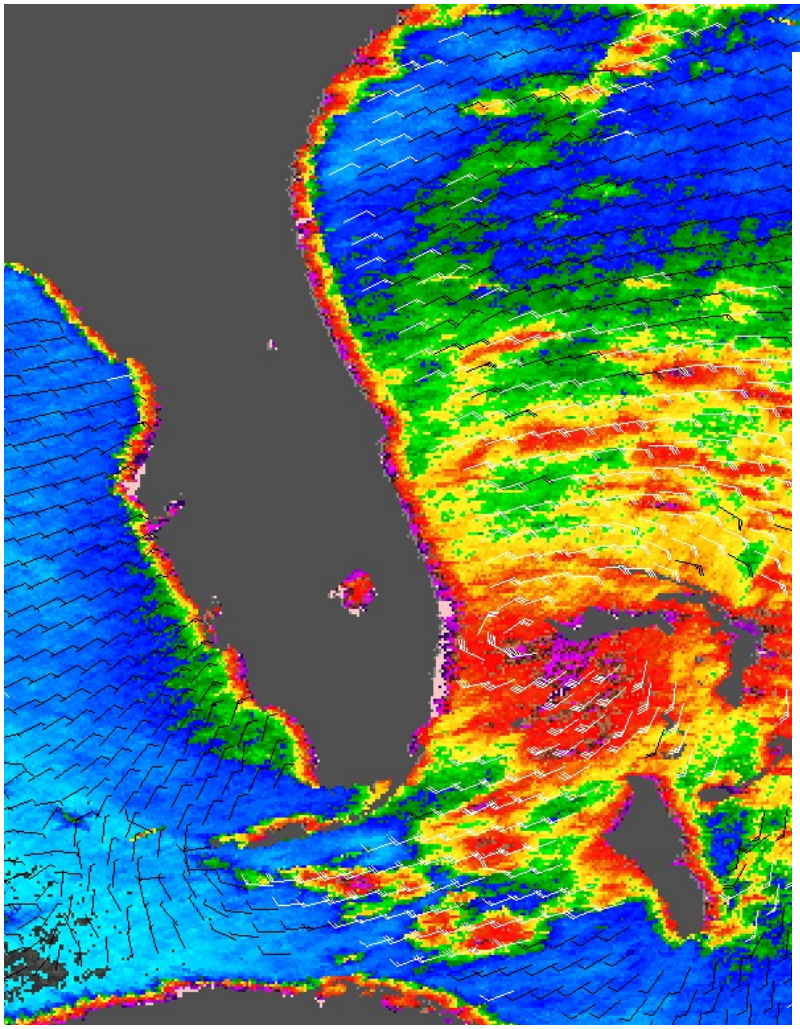

August 25, 2005,
Hurricane Katrina

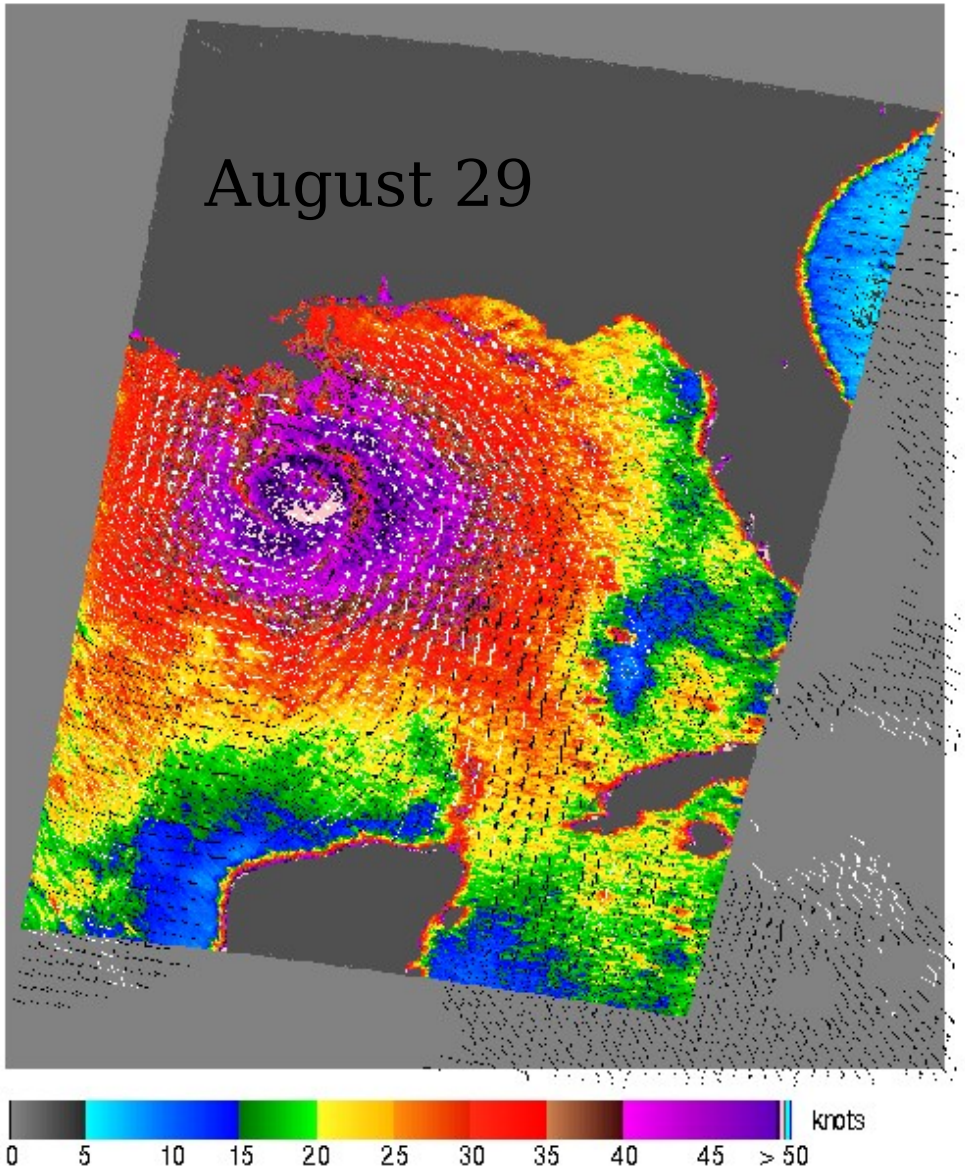

50Knots=57.6MPH; 10Knots ~ 18.55km/hour; 5.2m/s
White barbs point to areas of heavy rain

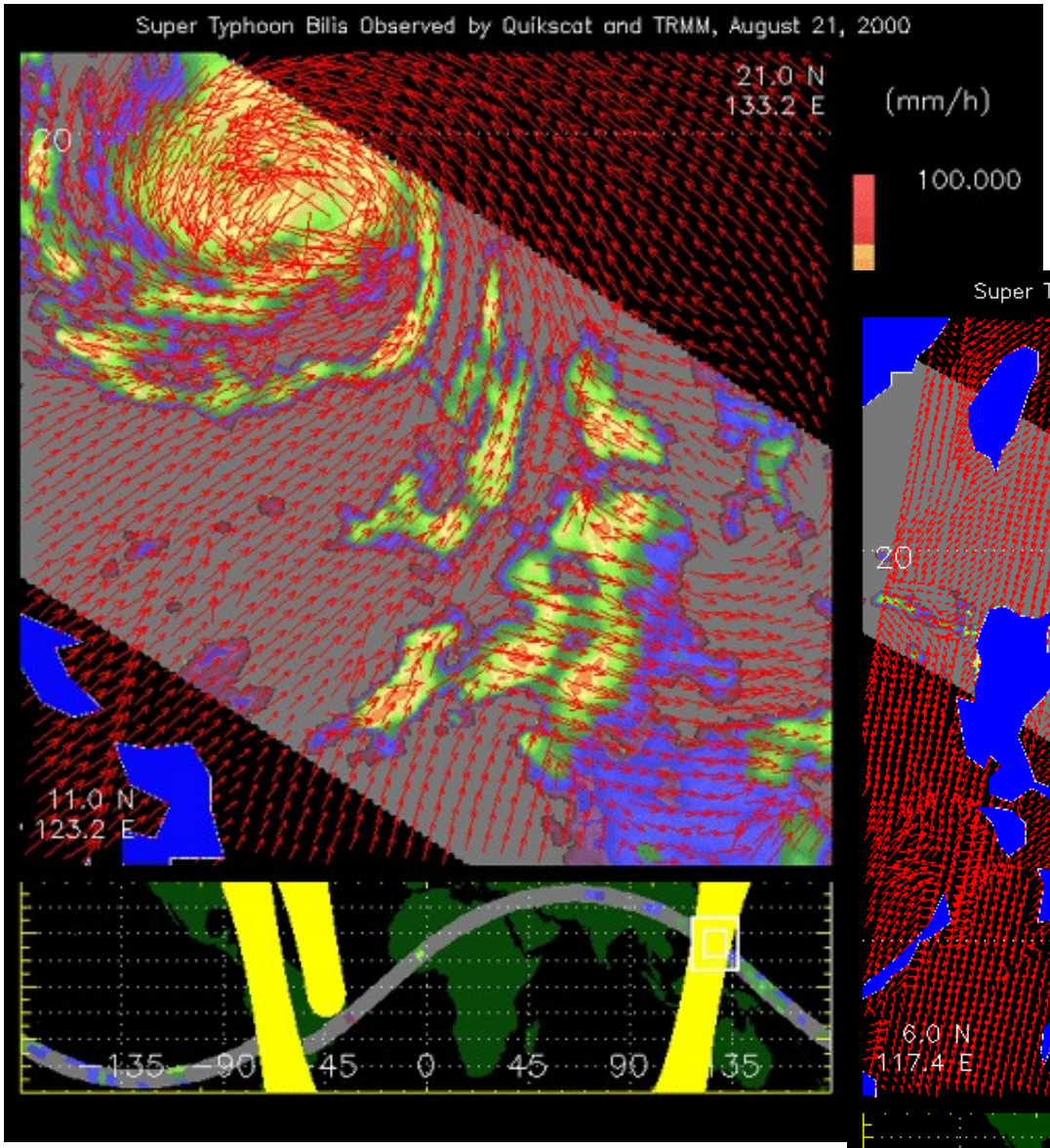
Super Typhoon Bilis Observed by Quikscat and TRMM, August 21, 2000
21.0 N
133.2 E
(mm/h)
100.000
20
11.0 N
123.2 E
135
90
45
0
45
90
135

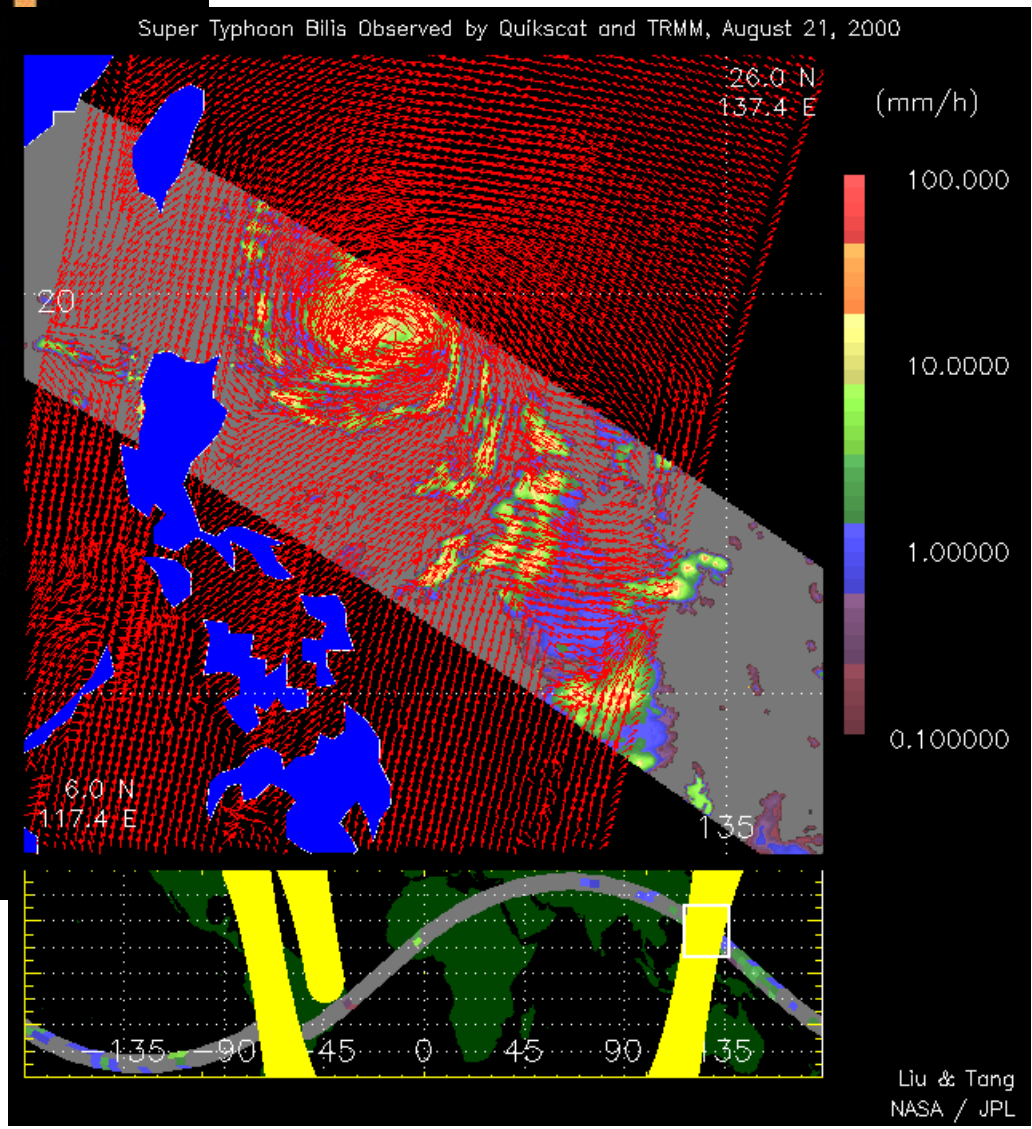
Super Typhoon Bilis Observed by Quikscat and TRMM, August 21, 2000
26.0 N
137.4 E
(mm/h)
100.000
10.0000
1.00000
0.100000
20
6.0 N
117.4 E
135
135
90
45
0
45
90
135
Liu & Tang
NASA / JPL

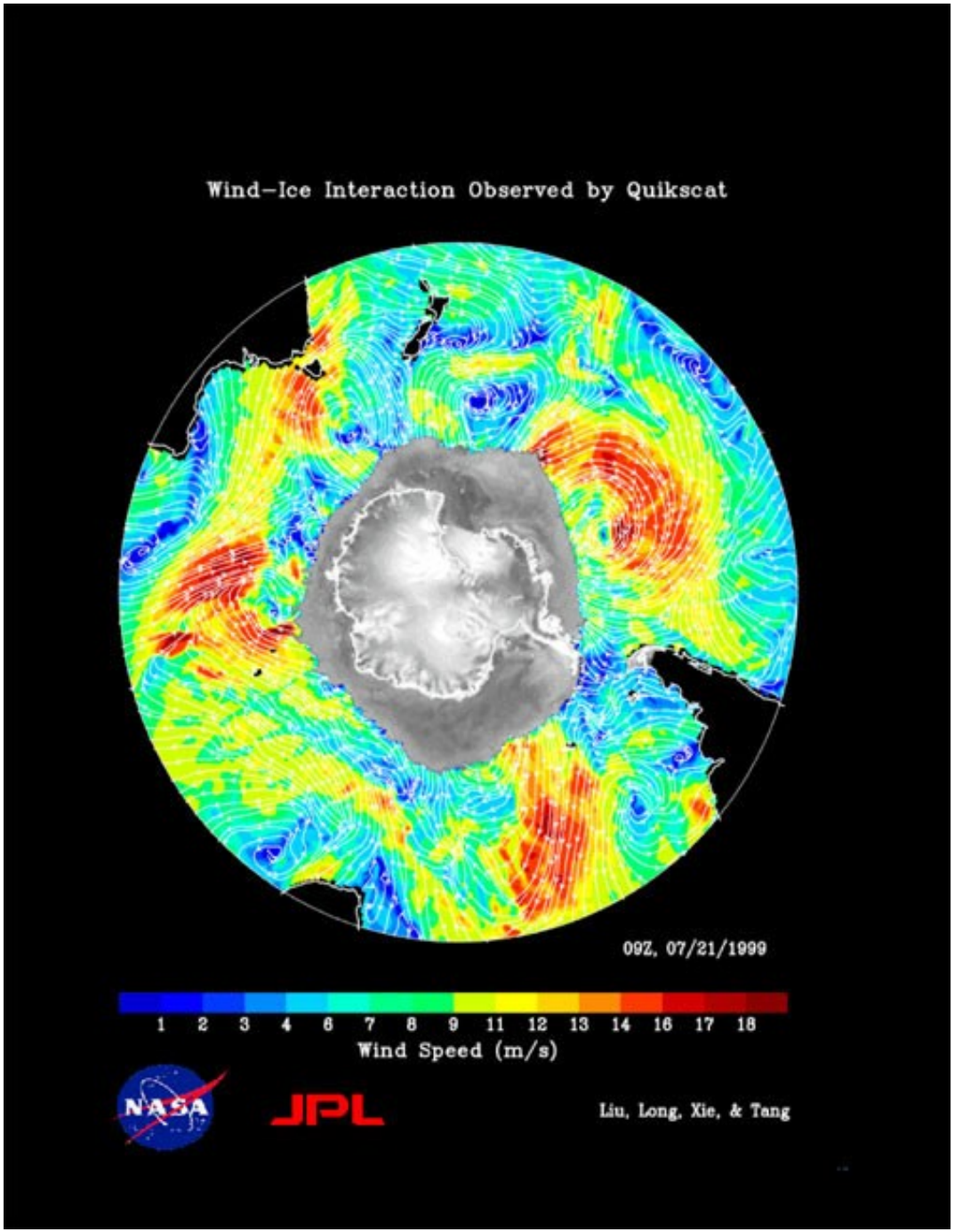
Wind–Ice Interaction Observed by Quikscat
09Z, 07/21/1999
1 2 3 4 6 7 8 9 11 12 13 14 16 17 18
Wind Speed (m/s)
NASA
JPL
Liu, Long, Xie, & Tang

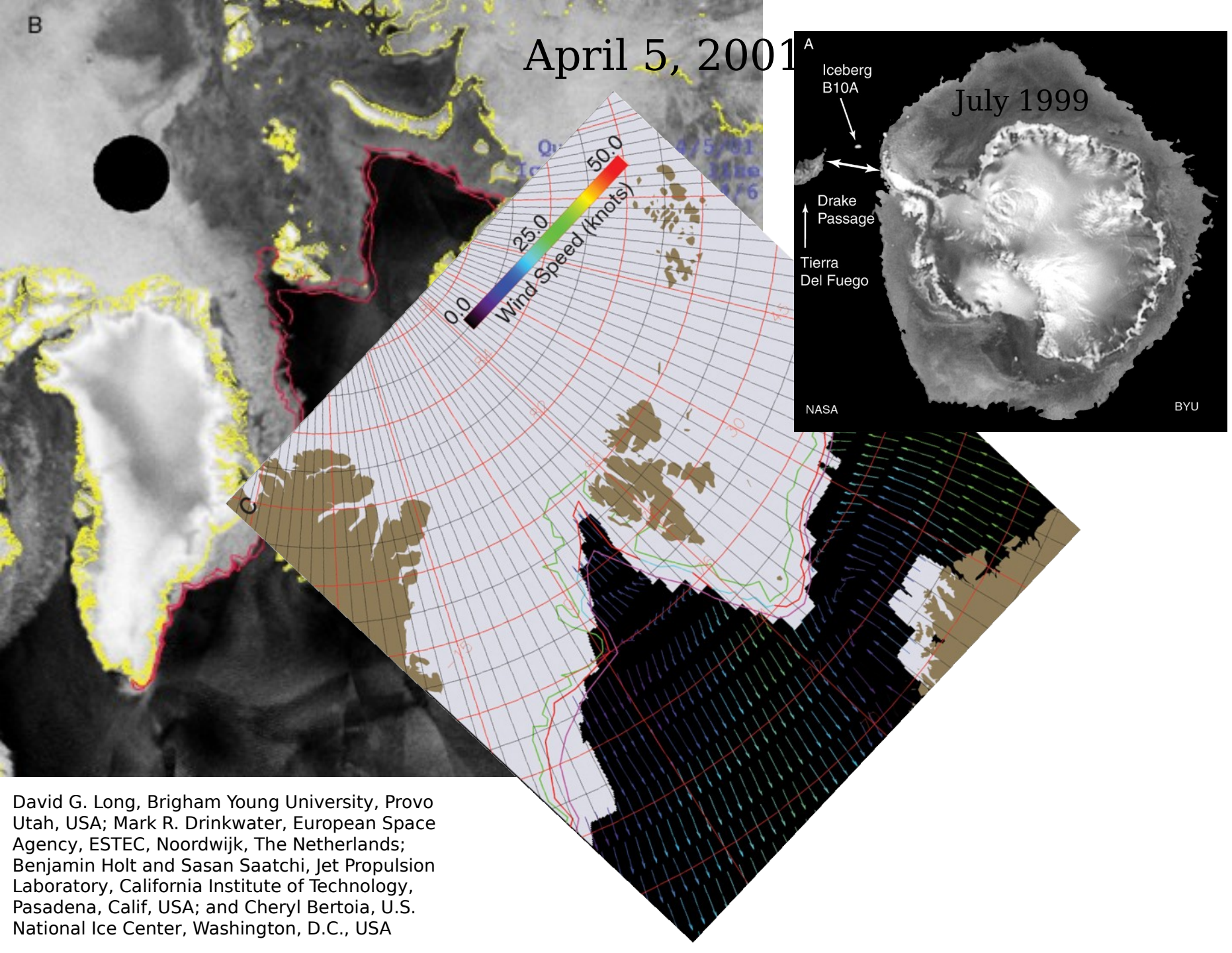

David G. Long, Brigham Young University, Provo Utah, USA; Mark R. Drinkwater, European Space Agency, ESTEC, Noordwijk, The Netherlands; Benjamin Holt and Sasan Saatchi, Jet Propulsion Laboratory, California Institute of Technology, Pasadena, Calif, USA; and Cheryl Bertoia, U.S. National Ice Center, Washington, D.C., USA

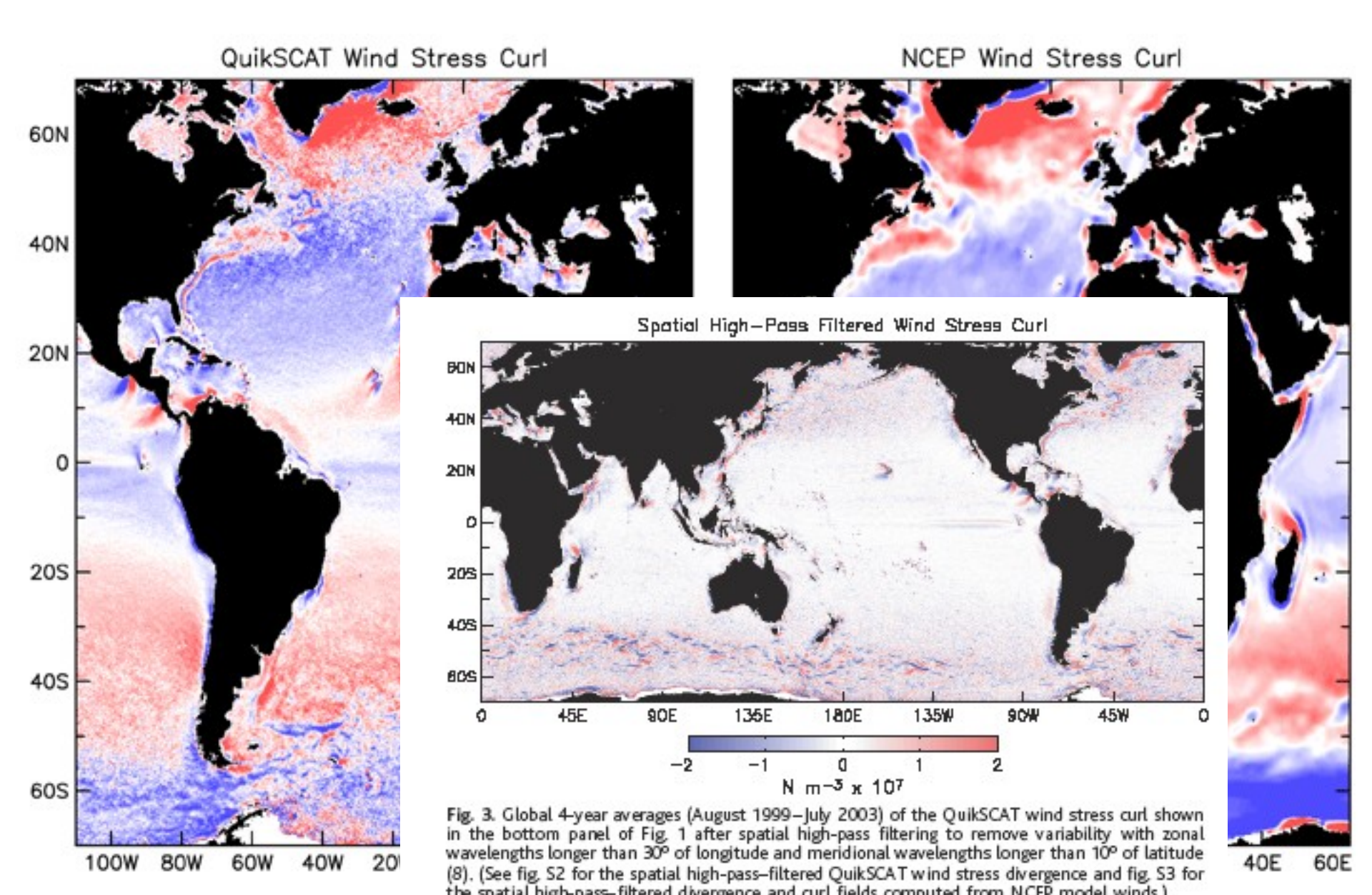

Fig. 3. Global 4-year averages (August 1999–July 2003) of the QuikSCAT wind stress curl shown in the bottom panel of Fig. 1 after spatial high-pass filtering to remove variability with zonal wavelengths longer than 30° of longitude and meridional wavelengths longer than 10° of latitude (*8*). (See fig. S2 for the spatial high-pass–filtered QuikSCAT wind stress divergence and fig. S3 for the spatial high-pass–filtered divergence and curl fields computed from NCEP model winds.)

Chelton, et al 2004

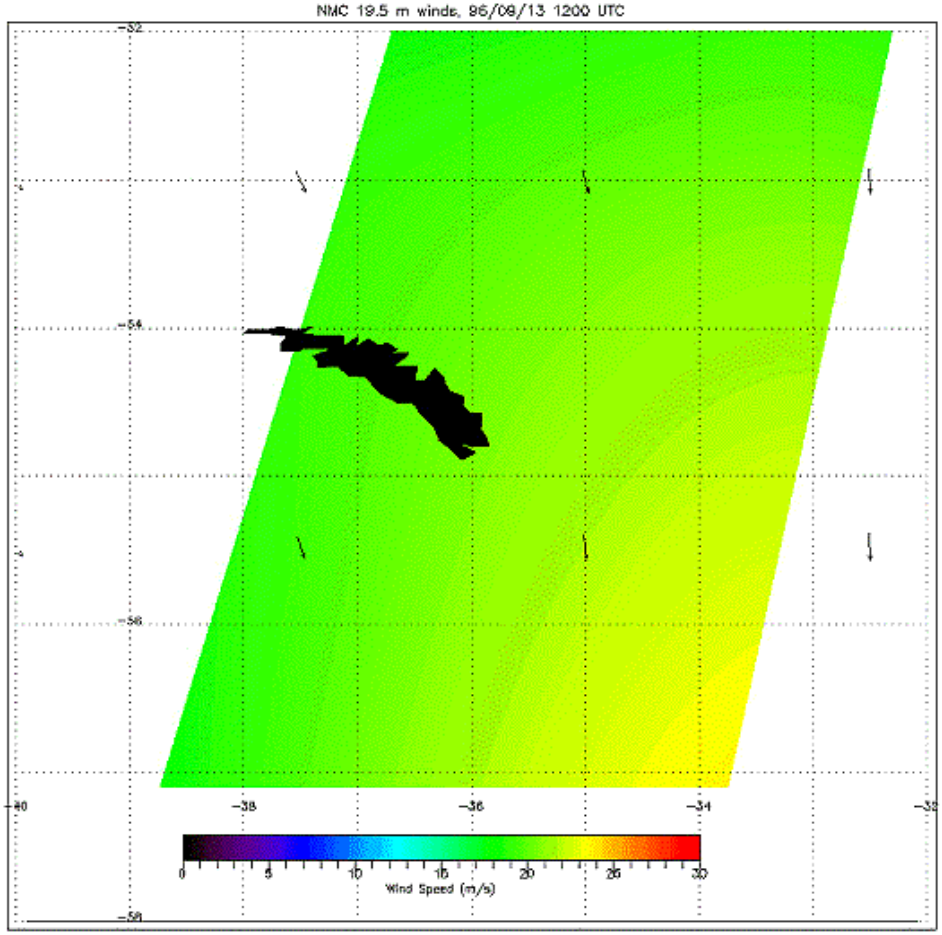
NMC 19.5 m winds, 96/09/13 1200 UTC
-32
-34
-36
-38
-40
-58
0
5
10
15
20
25
30
Wind Speed (m/s)

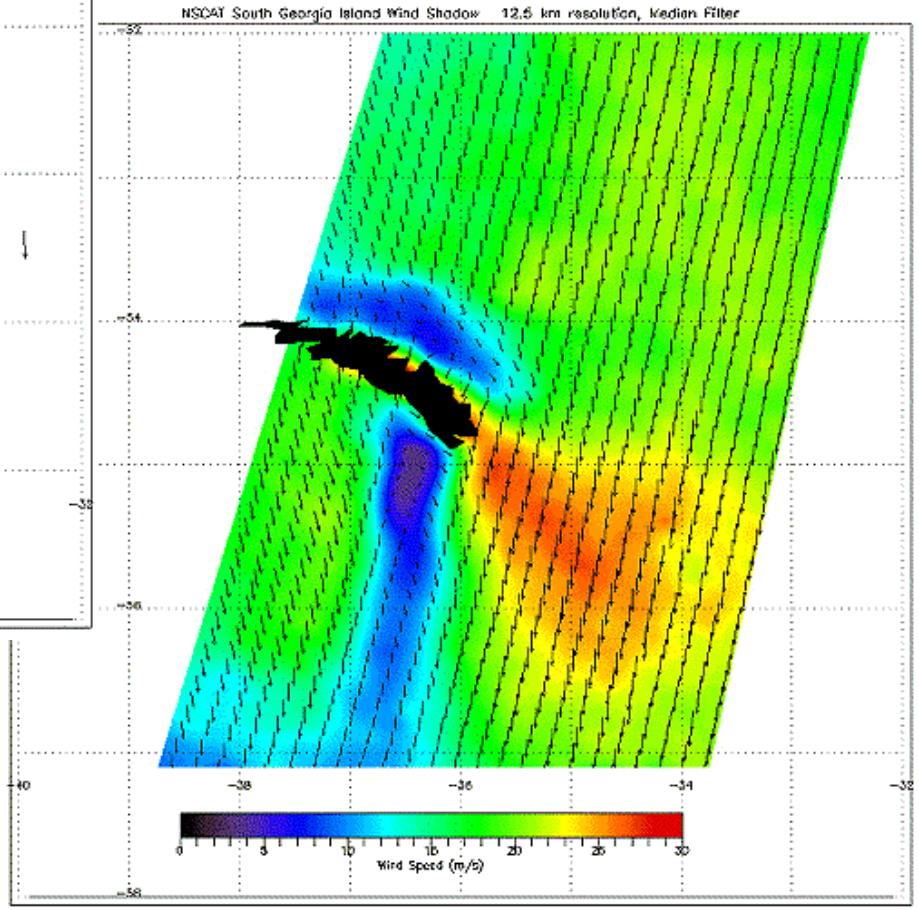
NSCAT South Georgia Island Wind Shadow 12.5 km resolution, Median Filter
-32
-34
-36
-38
-40
-58
0
5
10
15
20
25
30
Wind Speed (m/s)

Surface pressure fields … from scatterometer measureme

Brown & Patoux 2004 http://pbl.atmos.washington.edu/

$U_{10}/u^* = F(z, z_o, \text{stratification...})$

$U_{Geostrophic}/u^* = F(z, z_o, \text{stratification}, \lambda, \text{.....})$

$$\mathbf{U_G = \nabla P / (\rho f)}$$

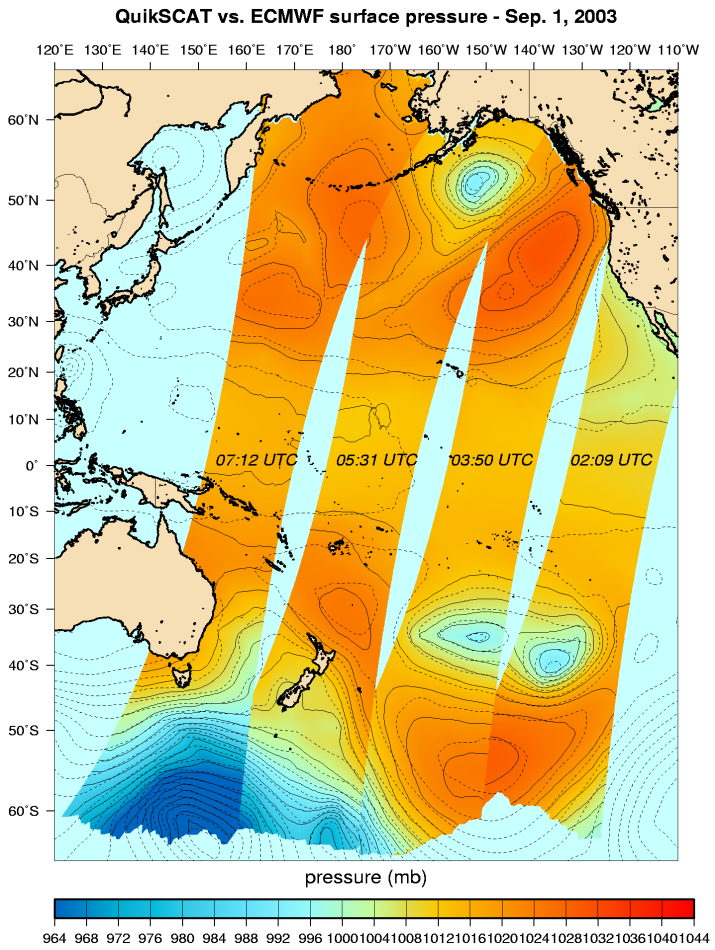

21 Jul 1999 - 00:00 UTC

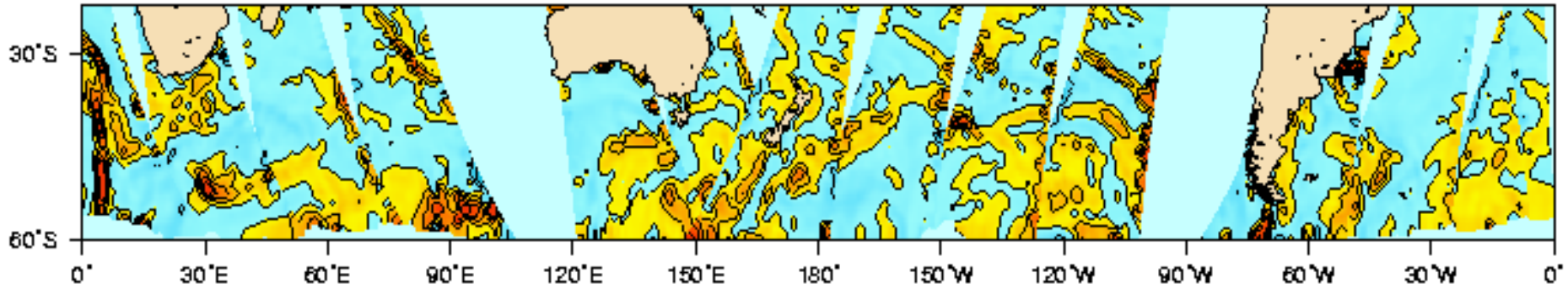

Divergence

Surface pressure

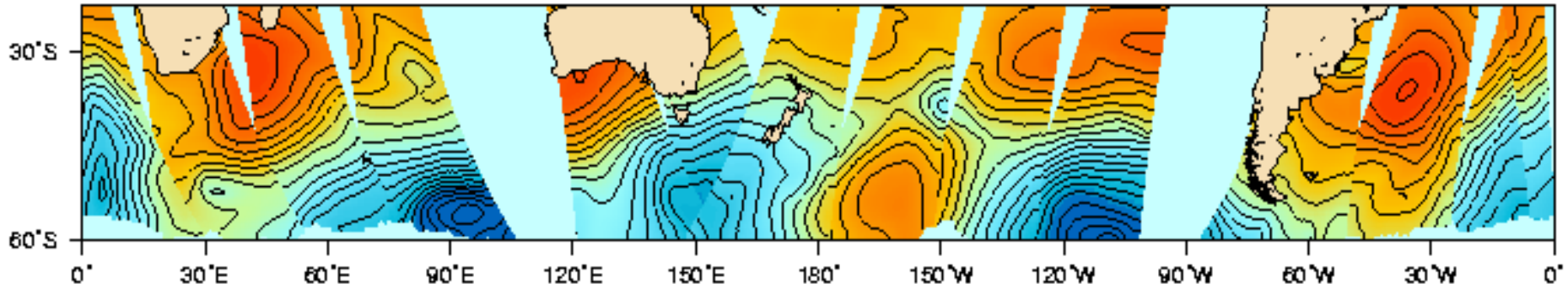

Patoux (2002)

Interesting Scatterometer sites:

NASA Scatterometer Data

Scatterometer Missions

“NASA's Quick Scatterometer (QuikSCAT) was lofted into space at 7:15 p.m. Pacific Daylight Time on Saturday (6/19/99) atop a U.S. Air Force Titan II launch vehicle from Space Launch Complex 4 West at California's Vandenberg Air Force Base. The satellite was launched in a south-southwesterly direction, soaring over the Pacific Ocean at sunset as it ascended into space to achieve an initial elliptical orbit with a maximum altitude of about 800 kilometers (500 miles) above Earth's surface.”

New Scatterometer SeaWinds on QuickSCAT

And Data